

ARTICLE

Platelets orchestrate the resolution of pulmonary inflammation in mice by T reg cell repositioning and macrophage education

Jan Rossaint¹, Katharina Thomas¹, Sina Mersmann¹, Jennifer Skupski¹, Andreas Margraf¹, Tobias Tekath², Charlotte C. Jouvencé³, Jesmond Dalli³, Andres Hidalgo⁴, Sven G. Meuth⁵, Oliver Soehnlein^{6,7,8}, and Alexander Zarbock¹

Beyond hemostasis, platelets actively participate in immune cell recruitment and host defense, yet their potential in the resolution of inflammatory processes remains unknown. Here, we demonstrate that platelets are recruited into the lung together with neutrophils during the onset of inflammation and alongside regulatory T (T reg) cells during the resolution phase. This partnering dichotomy is regulated by differential adhesion molecule expression during resolution. Mechanistically, intravascular platelets form aggregates with T reg cells, a prerequisite for their recruitment into the lung. This interaction relies on platelet activation by sCD40L and platelet P-selectin binding to PSGL-1 on T reg cells. Physical platelet-T reg cell interactions are necessary to modulate the transcriptome and instruct T reg cells to release the anti-inflammatory mediators IL-10 and TGFβ. Notably, the presence of platelet-T reg cell aggregates in the lung was also required for macrophage transcriptional reprogramming, polarization toward an anti-inflammatory phenotype, and effective resolution of pulmonary inflammation. Thus, platelets partner with successive immune cell subsets to orchestrate both the initiation and resolution of inflammation.

Introduction

Timely resolution of inflammation is important to impede uncontrolled host tissue destruction, and neutrophils need to be efficiently removed after clearance of the invading microorganisms to avoid excessive tissue damage (Arienti et al., 2019; Levy and Serhan, 2014). Neutrophil apoptosis with subsequent engulfment by macrophages is the major route by which the host clears neutrophils. Efficient phagocytosis of apoptotic neutrophils by macrophages (efferocytosis) not only prevents their secondary necrosis but also turns pro-inflammatory macrophages into cells with an anti-inflammatory, reparative signature (Doran et al., 2020). Dysfunction in the neutrophil apoptosis machinery is considered critical for the pathogenesis of many chronic human inflammatory diseases, e.g., pulmonary fibrosis after the acute respiratory distress syndrome (ARDS; Potey et al., 2019).

ARDS with accompanying pulmonary inflammation is a common life-threatening disease (Matthay et al., 2012). Despite

improved supportive care, the mortality rate of ARDS remains high and may reach up to 45% in severe ARDS (Ranieri et al., 2012). This syndrome may develop in response to several causes, including direct injury of the lung by bacterial or viral infection or aspiration of gastric content, or due to indirect causes, such as sepsis (Matthay et al., 2012). Pulmonary inflammation is characterized by an increased number of neutrophils in the lung and increased permeability, leading to lung edema and, consequently, decreased pulmonary gas exchange (Matthay et al., 2012; Semple et al., 2019). Indeed, neutrophil activation and recruitment participating in host defense are key events in the development of pneumonia and ARDS (Grommes and Soehnlein, 2011; Rebetz et al., 2018). Recruitment of neutrophils into inflamed tissue is required for eliminating invading pathogens, but can also cause tissue destruction by releasing a variety of enzymes and toxic granule content (Phillipson and Kubes, 2011).

¹Department of Anesthesiology, Intensive Care and Pain Medicine, University Hospital Münster, Münster, Germany; ²Institute of Medical Informatics, University of Münster, Münster, Germany; ³William Harvey Research Institute, Barts and The London School of Medicine and Dentistry, Queen Mary University of London, London, UK; ⁴Area of Cell and Developmental Biology, Fundación Centro Nacional de Investigaciones Cardiovasculares Carlos III, Madrid, Spain; ⁵Clinic of Neurology with Institute of Translational Neurology, University Hospital Münster, Münster, Germany; ⁶Institute for Experimental Pathology, Center for Molecular Biology of Inflammation, University of Münster, Münster, Germany; ⁷Department of Physiology and Pharmacology, Karolinska Institutet, Stockholm, Sweden; ⁸Institute for Cardiovascular Prevention, Ludwig-Maximilians-Universität München, Munich, Germany.

Correspondence to Alexander Zarbock: zarbock@uni-muenster.de.

© 2021 Rossaint et al. This article is distributed under the terms of an Attribution–Noncommercial–Share Alike–No Mirror Sites license for the first six months after the publication date (see <http://www.rupress.org/terms/>). After six months it is available under a Creative Commons License (Attribution–Noncommercial–Share Alike 4.0 International license, as described at <https://creativecommons.org/licenses/by-nc-sa/4.0/>).

The pathogenesis of pulmonary inflammation has been shown to be additionally platelet dependent in several lung injury models (Kornerup et al., 2010; Looney et al., 2009; Rossaint et al., 2014; Sreeramkumar et al., 2014; Zarbock et al., 2006). Platelet–neutrophil aggregates can be found in the lung microvasculature during pulmonary inflammation (Grommes et al., 2012; Rossaint et al., 2014; Zarbock et al., 2006), and the exchange of mediators between these two cell types amplifies inflammation (Rossaint et al., 2016). While it is now commonly accepted that the interaction of platelets and neutrophils is a prerequisite for neutrophil recruitment in many entities of ARDS, it remains unclear whether this interaction is restricted to the intravascular compartment or rather extends its influence in the tissue parenchyma. Beyond the importance for intravascular platelets for neutrophil recruitment, recent studies showed that platelet–neutrophil complexes are dynamically formed in the blood during pulmonary inflammation and that these complexes can also be found in the intra-alveolar space, thus indicating a role for intra-alveolar platelets in the pathogenesis of ARDS (Amison et al., 2018; Ortiz-Muñoz et al., 2014). It has been shown that macrophages are involved in the initial inflammatory phase of ARDS, but recent reports demonstrated that these cells are also involved in the resolution of pulmonary inflammation (Kapur et al., 2019). Regulatory T (T reg) cells represent a T cell subpopulation with predominantly immune regulatory functions and are immunosuppressive. T reg cells are a source of anti-inflammatory cytokines IL-10 and TGF β . T reg cells have been shown to exert anti-inflammatory functions during the onset of lung injury with IL-10 playing an important role (Kapur et al., 2017a), and low IL-10 levels may represent a risk factor for the development of ARDS (Kapur et al., 2017b). Here, IL-2 appears to be a protective mediator triggering IL-10 release by T reg cells as a counterbalance in acute inflammation (e.g., TRALI; He et al., 2019); however, whether and how platelets, macrophages, and T reg cells may cooperate during the resolution of pulmonary inflammation is unknown.

The aim of the present study was to investigate the role of platelets during inflammation resolution and to identify cellular partners involved in this process. We find that intravascular platelets are crucially required for the recruitment of T reg cells into the lung and that intra-alveolar platelet relocation is indispensable for macrophage polarization toward an anti-inflammatory phenotype, aiding in the clearance of alveolar neutrophils and termination of pulmonary inflammation.

Results

Platelets are required for the clearance of intra-alveolar neutrophils

Bacterial pneumonia represents clinically the most important etiology of ARDS. Therefore, we chose the infectious model of bacterial-induced pneumonia for this study (Cilloniz et al., 2018). Platelets are required for neutrophil recruitment into the lung during pneumonia (Rossaint et al., 2016). After induction of bacterial pneumonia, neutrophil recruitment into the alveoli, accompanied by increased MIP2 α serum levels, plateaued at day 2 and declined subsequently (Fig. 1 A and Fig. S1 A).

To assess time dependency, we depleted platelets by intravascular injection of a platelet-targeting α -GPIb α antibody at day 2 (i.e., after peak neutrophil recruitment), which lead to a reduction of >98% of circulating platelets over a period of 3 d (Fig. S1 B). Alveolar neutrophil numbers remained high on days 4 and 5 in platelet-depleted mice (Fig. 1 A). Additionally, we used Pf4^{iDTR} mice (Pf4Cre;Rosa^{iDTR} mice) to selectively deplete platelets (Fig. 1 A; Wuescher et al., 2015). We chose to start diphtheria toxin (DT) treatment 3 d before pneumonia induction to match depletion and the peak of neutrophils in the lung (Fig. S1 C). DT administration did not affect the blood counts of erythrocytes or leukocyte subsets (Fig. S1 D). In Pf4^{iDTR} mice, the number of alveolar neutrophils also remained high on days 4 and 5 (Fig. 1 A). If platelets were depleted before the induction of bacterial pneumonia, all mice died within a 48 h of observation period due to abolished, initial neutrophil recruitment and overwhelming bacterial dissemination (Fig. S1 E). Neutrophil apoptosis in the bronchoalveolar lavage (BAL) remained low in Pf4^{iDTR} and platelet-depleted mice until day 5 compared with elevated apoptosis in control mice (Fig. 1 B). Consistently, we observed that platelet depletion caused persistent high neutrophil counts and decreased neutrophil apoptosis in the lung interstitial space at day 5 (Fig. 1, C and D; for exemplary FACS plots, see Fig. S2 A) and increased lung wet/dry ratios (Fig. S1 F), which is altogether indicative of delayed resolution of inflammation in the absence of platelets. To assess whether continuing polymorphonuclear granulocyte (PMN) recruitment after day 2 following induction of pneumonia affects the balance between PMN influx and clearance in the lungs, we depleted PMNs by DT administration in Mrp8-iDTR mice on day 2 after pneumonia induction and observed similar counts of viable and apoptotic PMN in the BAL and lung interstitial compartment on days 3–5 as in the respective non-PMN-depleted groups (Fig. 1, A–D). Notably, the effects of platelet depletion on the counts of viable and apoptotic PMNs in the BAL and lung interstitial compartment on days 3–5 were comparable in control mice and PMN-depleted mice, thus showing that PMN clearance is the major determinant of net PMN accumulation during the resolution of pulmonary inflammation in our model. To exclude that PMN-bound, activated platelets binding annexin V by surface-expressed phosphatidylserine falsely mimics PMN apoptosis, we analyzed CD41⁺ PMNs from control mice after pneumonia induction and could still observe similar apoptosis rates (Fig. S2 D).

Unresolved acute inflammation may lead to sustained, chronic inflammation in the lung, with increased deposition of collagen fibers in the lung (Levy and Serhan, 2014). The lack of platelets during the resolution phase (days 3–5) led to a significantly increased collagen content and reduced lung compliance of the lung after 2 wk of pneumonia induction (Fig. 1, E and F). This was reversed by intratracheal (i.t.) instillation of 5,6-dichloro-1- β -D-ribofuranosylbenzimidazole (DRB), a specific cyclin-dependent kinase 7/9 inhibitor that induces neutrophil apoptosis in the lung after i.t. instillation (Leitch et al., 2012; Rossi et al., 2006). Histological analysis showed persistent pulmonary inflammation, fibrotic tissue remodeling, and elevated Ashcroft scores (Ashcroft et al., 1988) in platelet-depleted

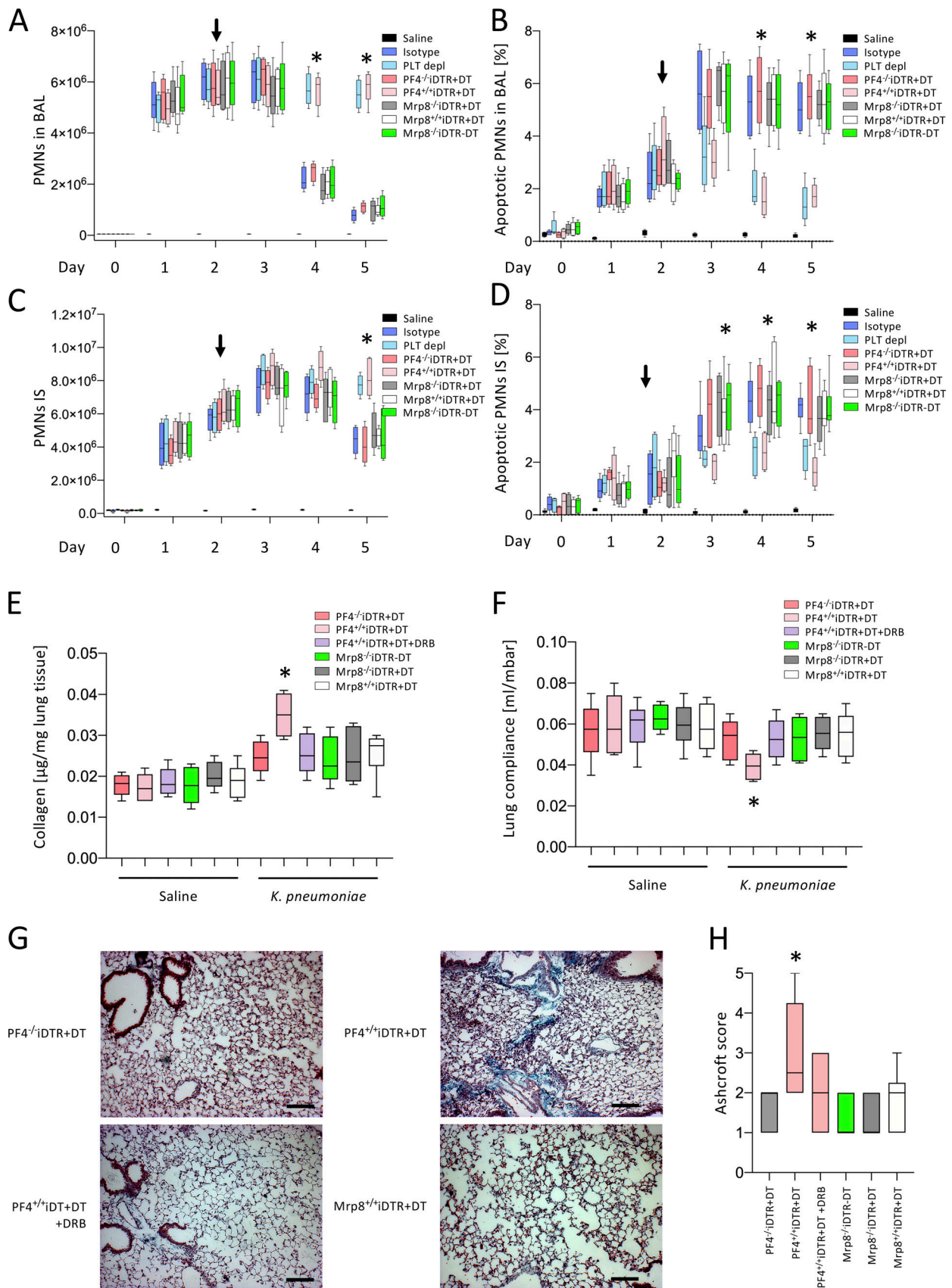


Figure 1. **Platelets are required for the clearance of intra-alveolar neutrophils.** Bacterial pneumonia was induced in WT, PF4^{+/-}iDTR+DT, PF4^{-/-}iDTR+DT, Mrp8^{+/-}iDTR+DT, Mrp8^{-/-}iDTR+DT, and Mrp8^{-/-}iDTR-DT mice by i.t. instillation of viable *K. pneumoniae* (1.5×10^7 CFU/mouse). WT mice received a platelet-depleting

antibody (clone R300, 2 $\mu\text{g/g}$ body weight) or isotype control IgG 2 d after induction of pneumonia. All conditional iDTR mice were treated with DT (+DT) on day 2. **(A and B)** The number of neutrophils in the BAL fluid (A) and the percentage of apoptotic neutrophils in the BAL (B) was analyzed by flow cytometry (data pooled from at least two independent experiments with four to six mice in each group; Mann-Whitney test was used for statistical analysis, *, $P < 0.05$). Arrows indicate time point of platelet depletion. **(C and D)** Likewise, the number of neutrophils in the interstitial space (IS; C) and the percentage of apoptotic neutrophils in the interstitial space (D) was analyzed (data pooled from at least two independent experiments with four to six mice in each group; Mann-Whitney test was used for statistical analysis, *, $P < 0.05$). **(E and F)** 14 d after induction of pneumonia, lung collagen content (estimated by measuring the absorbance of oxidized hydroxyproline in lung tissue homogenisates; E) and lung compliance (F) were analyzed in PF4^{-/-}iDTR+DT mice and in PF4^{+/+}iDTR+DT mice with or without DRB, Mrp8^{+/+}iDTR+DT, Mrp8^{-/-}iDTR+DT, and Mrp8^{-/-}iDTR-DT (data pooled from at least two independent experiments with four to six mice in each group; Mann-Whitney test was used for statistical analysis, *, $P < 0.05$). **(G)** Exemplary histological images of Masson-Goldner staining of DRB-treated PF4^{-/-}iDTR+DT and PF4^{+/+}iDTR+DT as well as Mrp8^{+/+}iDTR+DT mice to visualize collagen fiber (blue) deposition. Scale bar, 100 μm . **(H)** Histological lung fibrosis was quantified using the Ashcroft scoring system (data pooled from at least two independent experiments with four to six mice in each group; Mann-Whitney test was used for statistical analysis, *, $P < 0.05$).

mice after 2 wk (Fig. 1, G and H). In comparison, neutrophil depletion prevented fibrotic tissue remodeling (Fig. 1, G and H). These data demonstrated an unexpected and absolute requirement for platelets during the resolution phase of pulmonary inflammation.

Platelets differentially bind to neutrophils and T reg cells at distinct time points of an inflammatory response

T reg cells are recruited into the lung during the resolution of inflammation (Ehrentraut et al., 2013). Platelet–neutrophil aggregates in peripheral blood were rapidly detectable and their frequency steadily decreased from day 2, whereas platelet–T reg cell aggregates were first detected after 2 d and steadily increased until day 5, corresponding to the resolution phase (Fig. 2, A–C; for exemplary FACS plots, see Fig. S2, B and C). Platelet interactions with monocytes and CD4 T cells did not show significant alterations, whereas the percentage of CD41⁺ CD8 cells slightly increased on day 5 following the induction of pulmonary inflammation (Fig. 2 A). T reg cell counts in blood increased after 2 d (Fig. 2 D), and T reg cell recruitment in lungs started 2–3 d after pneumonia induction and was nearly completely abolished following platelet depletion at day 2 (Fig. 2 E). To address this dichotomous behavior and the switch from platelets preferably binding to neutrophils during the onset of inflammation toward mainly binding T reg cells during the resolution phase, we analyzed the surface expression of adhesion molecules on neutrophils, platelets, and T reg cells. Interestingly, PSGL-1 and Mac-1 expression on circulating neutrophils significantly decreased after the onset of pulmonary inflammation following day 2 (Fig. 2, F and G), while the surface expression of the counter receptors P-selectin and GPIb, respectively, on platelets remained steady after initial inflammatory stimulus (P-selectin; Fig. 2 H) or unaltered, as in the case of GPIb (Fig. 2 I). In contrast, expression of PSGL-1 (Fig. 2 J) on circulating T reg cells was increased 2 d after pneumonia, suggesting that this was the rate-limiting step in platelet binding. The sheddase ADAM8 is externalized by neutrophils following activation and aids in the migration through the lung tissue (Dreymueller et al., 2017), but cleaves PSGL-1 on neutrophils (Domínguez-Luis et al., 2011). Circulating neutrophils showed an increase of ADAM8 expression 3 d after pneumonia induction compared with noninfected mice (Fig. 2 K). Incubation of isolated neutrophils with rADAM8 (300 pg/ml) inhibited platelet–neutrophil aggregate formation

to a level similar to PSGL-1 blockade (Fig. 2 L), and blocking ADAM8 activity (inhibitor BK-1361, 25 $\mu\text{g/g}$ body weight) preserved the prevalence of platelet–neutrophil aggregates in vivo (Fig. 2 M), whereas platelet–T reg cell interactions remained unaltered (Fig. 2 N). Thus, there appears to be a molecular transition from platelets preferentially binding to neutrophils early during inflammation, whereby ADAM8 cleaves PSGL-1 and allows the preferential binding of platelets to T reg cells during the resolution phase. ADP (adenosine diphosphate) is a weak platelet agonist and it has been published that ADP induces a dose-dependent release of platelet α -granules and increases platelet P-selectin surface expression in a dose-dependent manner (Dong et al., 2015; Elaib et al., 2016; Lu et al., 2015), which we also observed in dose-response experiments in vitro (Fig. S2, F and G).

Platelets regulate IL-10 and TGF β cytokine homeostasis and guide T reg cells to inflamed alveoli

The effect of intravascular platelet depletion on neutrophil clearance from the lung at day 2 after onset of initial neutrophil accumulation suggested the imminent importance of platelets entering the alveoli at a later time point. Thus, we injected WT mice with red fluorescent platelets isolated from DsRed⁺ mice at day 3 after pneumonia induction. We detected red fluorescent platelets in the BAL fluid on day 5 (Fig. 3 A), indicating that, although neutrophil recruitment into the lung did not continue after day 2, platelets still translocated into the alveoli with similar ratios of WT to DsRed⁺ platelets in the blood and BAL (Fig. 3, B and C). Analysis of the platelet activation status in the BAL revealed platelets in the BAL to, at least in part, express P-selectin on their surface (Fig. S2 H). In a reciprocal experiment, we injected isolated DsRed⁺ platelets i.v. into WT mice before induction of pneumonia and found progressive decline in the BAL fluid up to day 5 (Fig. 3 C). We next transferred platelets (10^8 to 5×10^8 platelets/mouse) into platelet-depleted mice to determine whether this could rescue normal leukocyte dynamics. Platelet-reconstituted Pf4^{iDTR} mice displayed a concentration-dependent rescue of pulmonary T reg cell recruitment (Fig. 3 D). The rationale for choosing day 3 for the platelet reconstitution was not to interfere with the role of platelets during the initiation phase of pulmonary inflammation or with the administration of platelet-depleting antibodies at day 2 after induction of pneumonia.

T reg cell recruitment coincided with the appearance of anti-inflammatory cytokines IL-10 and TGF β in the BAL starting from

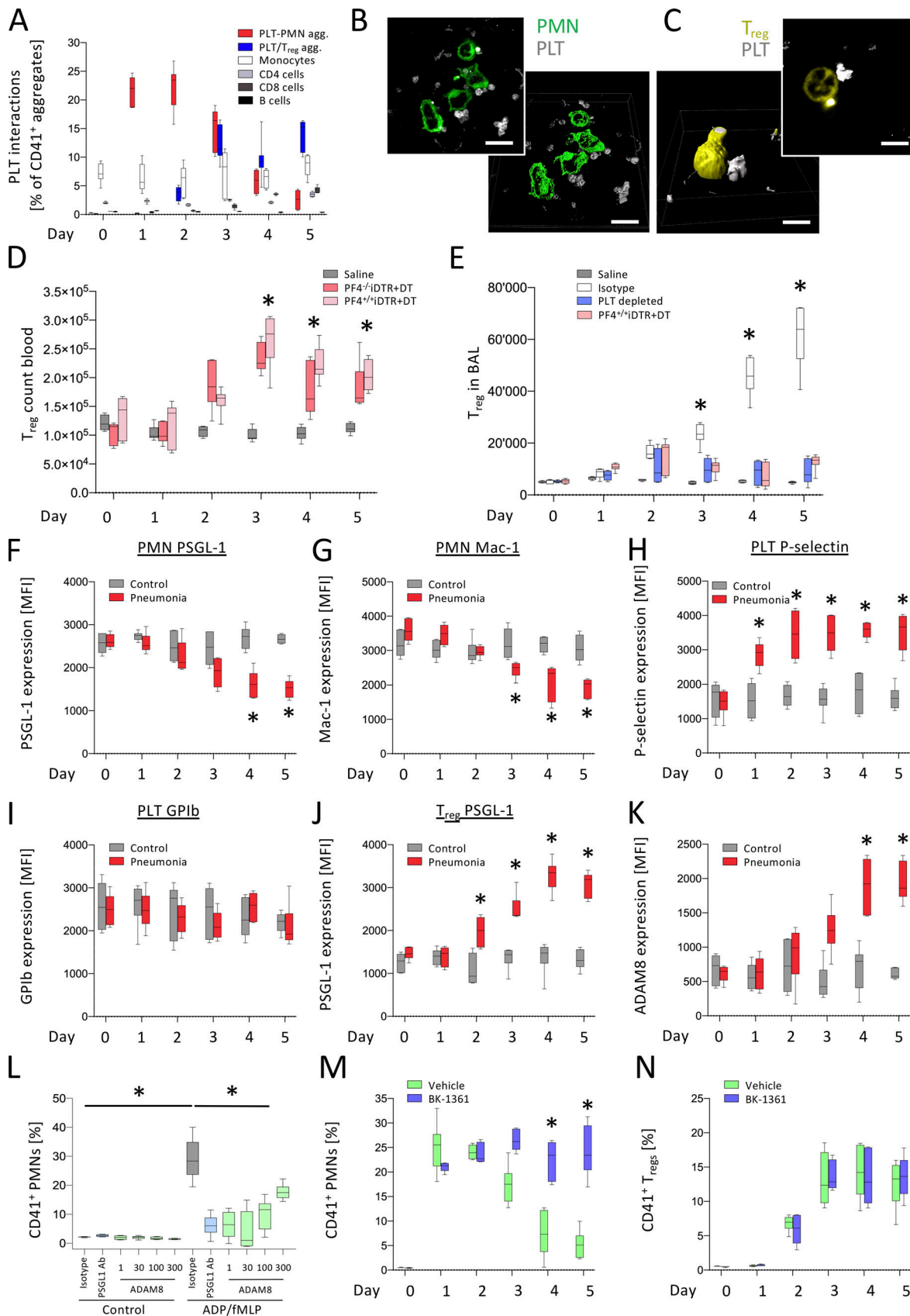


Figure 2. **Platelets differentially bind to neutrophils and T reg cells at distinct time points of an inflammatory response.** Bacterial pneumonia was induced in WT mice and PF4^{+/+}iDTR+DT (receiving DT) mice by i.t. instillation of viable *K. pneumoniae* (1.5×10^7 CFU/mouse). Some mice received a platelet-depleting antibody (clone R300, 2 μ g/g body weight) or isotype control 2 d after induction of pneumonia. **(A)** Platelet–neutrophil and platelet–T reg cell

aggregates in the circulation were analyzed by flow cytometry. Data pooled from three independent experiments with four to six mice in each group (data pooled from at least two independent experiments with six samples in each group; Mann-Whitney test was used for statistical analysis, *, $P < 0.05$). **(B and C)** Immunofluorescence staining and 3D reconstruction of (B) platelet–neutrophil and (C) platelet–T reg cell aggregates in peripheral blood samples. Exemplary images are shown from at least two experimental repetitions. Scale bar, 10 μm . **(D)** Blood counts of T reg cells were analyzed by flow cytometry (data pooled from two independent experiments with four to five samples in each group; Mann-Whitney test was used for statistical analysis, *, $P < 0.05$). **(E)** The number of T reg cells in the BAL fluid was analyzed by flow cytometry (data pooled from two independent experiments with four to six samples in each group; Mann-Whitney test was used for statistical analysis, *, $P < 0.05$). Pneumonia was induced in WT mice by i.t. instillation of *K. pneumoniae* (data pooled from two independent experiments with four to six samples in each group; Mann-Whitney test was used for statistical analysis, *, $P < 0.05$). **(F–K)** The expression of (F) PSGL-1 and (G) Mac-1 on neutrophils, (H) P-selectin and (I) GPIb on single platelets, and (J) PSGL-1 on T reg cells and ADAM8 on neutrophils (K) was analyzed at the indicated time points (data pooled from at least two independent experiments with four to five samples in each group; Mann-Whitney test was used for statistical analysis, *, $P < 0.05$). **(L)** Isolated WT neutrophils were pretreated with a blocking PSGL-1 antibody (clone 4RA10, 5 $\mu\text{g}/\text{ml}$) or rADAM8 (1–300 pg/ml), coincubated with isolated WT platelets, and platelet–neutrophil aggregates were analyzed by flow cytometry (data pooled from two independent experiments with four to six samples in each group; Mann-Whitney test was used for statistical analysis, *, $P < 0.05$). **(M and N)** After induction of bacterial pneumonia animals were treated with BK-1361 (25 $\mu\text{g}/\text{g}$) and circulating platelet–neutrophil (M) platelet–T reg cell aggregates (N) were analyzed by flow cytometry at the indicated time points (data pooled from two independent experiments with six samples in each group; Mann-Whitney test was used for statistical analysis, *, $P < 0.05$). MFI, mean fluorescence intensity; PLT, platelet.

day 3 (Fig. 3, E and F; compare with Fig. 2 E). DT-mediated depletion of intravascular platelets in $\text{P}f4^{\text{IDTR}}$ mice, depletion of T reg cells in $\text{FoxP3}^{\text{DTR}}$ mice (DEREG mice; Fig. S3 A), as well as blocking of VLA-4 (an integrin required for T reg migration; Klann et al., 2018) all prevented the increase of IL-10 in the BAL (Fig. 3 E). Importantly, depletion of T reg cells by using DEREG mice did not cause neutrophil accumulation by itself (Fig. S3 B); however, upon induction of inflammation, T reg cell depletion caused persistently high neutrophil numbers in the BAL and decreased neutrophil apoptosis and platelet numbers in the BAL, both of which were reversed by T reg cell reconstitution or administration of recombinant IL-10 (Fig. 3, G and H). T reg cell depletion also led to increased lung collagen content and reduced lung compliance (Fig. 3, I and J). These data demonstrate that platelets drive the recruitment of T reg cells in the alveoli, which, in turn, contributes to resolve pulmonary inflammation.

Platelet–T reg cell interactions are required for pulmonary T reg cell recruitment and activation

T reg cells express CD40 ligand (CD40L), which is shed and released as soluble CD40L (sCD40L). Platelets express the counter receptor CD40 binding sCD40L, causing platelet activation. The integrins $\alpha_{\text{IIb}}\beta_3$ and $\alpha_5\beta_1$ expressed on the platelet surface then mediate platelet aggregation. We detected increased sCD40L plasma levels after pneumonia induction (Fig. 4 A). Similar sCD40L levels were detected in platelet-depleted mice, indicating that T reg cells rather than platelets themselves are the source of sCD40L in this condition (Fig. 4 A). Incubation of isolated WT platelets with sCD40L significantly increased platelet P-selectin surface expression levels, platelet fibrinogen binding, and shape change, as indicated by analysis of platelet spreading stages on serum-coated coverslips, indicating platelet activation (Fig. 4, B–D; and Fig. S3 C). Furthermore, CD40L stimulation caused mild platelet aggregation as detected by aggregometry (Fig. 4 E). Stimulation with sCD40L induced platelet–T reg cell aggregate formation in vitro, which was significantly decreased by pretreatment with a CD40-blocking antibody (Fig. 4 F). T reg cells express PSGL-1, the counter receptor for platelet P-selectin and a major determinant of platelet interaction with leukocytes (Rossaint and Zarbock, 2015; Sreeramkumar et al., 2014). Pretreatment with P-selectin or

PSGL-1-blocking antibodies significantly decreased platelet–T reg cell aggregate formation (Fig. 4 F). Coculture of T reg cells and platelets increased the release of IL-10 and $\text{TGF}\beta$, and the levels of both cytokines were reduced after blocking either P-selectin, PSGL-1, or CD40 (Fig. 4, G and H). Although supernatant from sCD40L-treated platelets contains $\text{TGF}\beta$, the incubation of isolated T reg cells with supernatant from sCD40L-treated platelets alone did not increase IL10 production by T reg cells (Fig. 4, G and H). These data suggest that direct platelet–T reg cell interactions elicit the production of anti-inflammatory cytokines. To investigate possible indirect effects of platelets on T reg cells, we coincubated isolated T reg cells with supernatant from activated platelets. We could neither detect alterations in IL-10 and $\text{TGF}\beta$ release by T reg cells, nor alteration in PSGL-1 expression, indicating that the effect of platelets on T reg cells is through direct cell–cell interactions (Fig. 4, G and H). These data further illustrate the switch in cellular partnership of platelets from neutrophils during the early inflammatory response to T reg cells in the late resolution phase.

Consistent with the requirement for cell–cell contacts mediated by P-selectin and CD40, the number of T reg cells recruited into the alveoli was significantly reduced by blocking either receptor by using F(ab) fragments after the initial recruitment phase, and accordingly the numbers of neutrophils in the BAL remained high until day 5 (Fig. 4, I and J). These treatments also significantly reduced apoptotic neutrophils and IL-10 and $\text{TGF}\beta$ concentrations in the BAL and led to increased collagen content and decreased lung compliance (Fig. S4, A–D). Blocking CD40–CD40L interactions before infection did not significantly affect neutrophil or T reg cell accumulation at day 3, nor modulated neutrophil apoptosis or IL-10 concentrations in the BAL at day 5, indicating that CD40–CD40L interactions are not relevant for the initial immune response to pneumonia infection (Fig. S4, E–H).

We next investigated the role of platelets on the differential regulation of the T reg cell transcriptome. We induced pulmonary inflammation and isolated T reg cells alone and platelet–T reg cell aggregates from the BAL at day 5. For this purpose, the single platelet transcriptome was deducted from the platelet–T reg cell transcriptome. Direct platelet–T reg cell interactions caused the differential expression of 1,897 genes in T reg cells compared with T reg cells without bound platelets (Fig. 4, K and

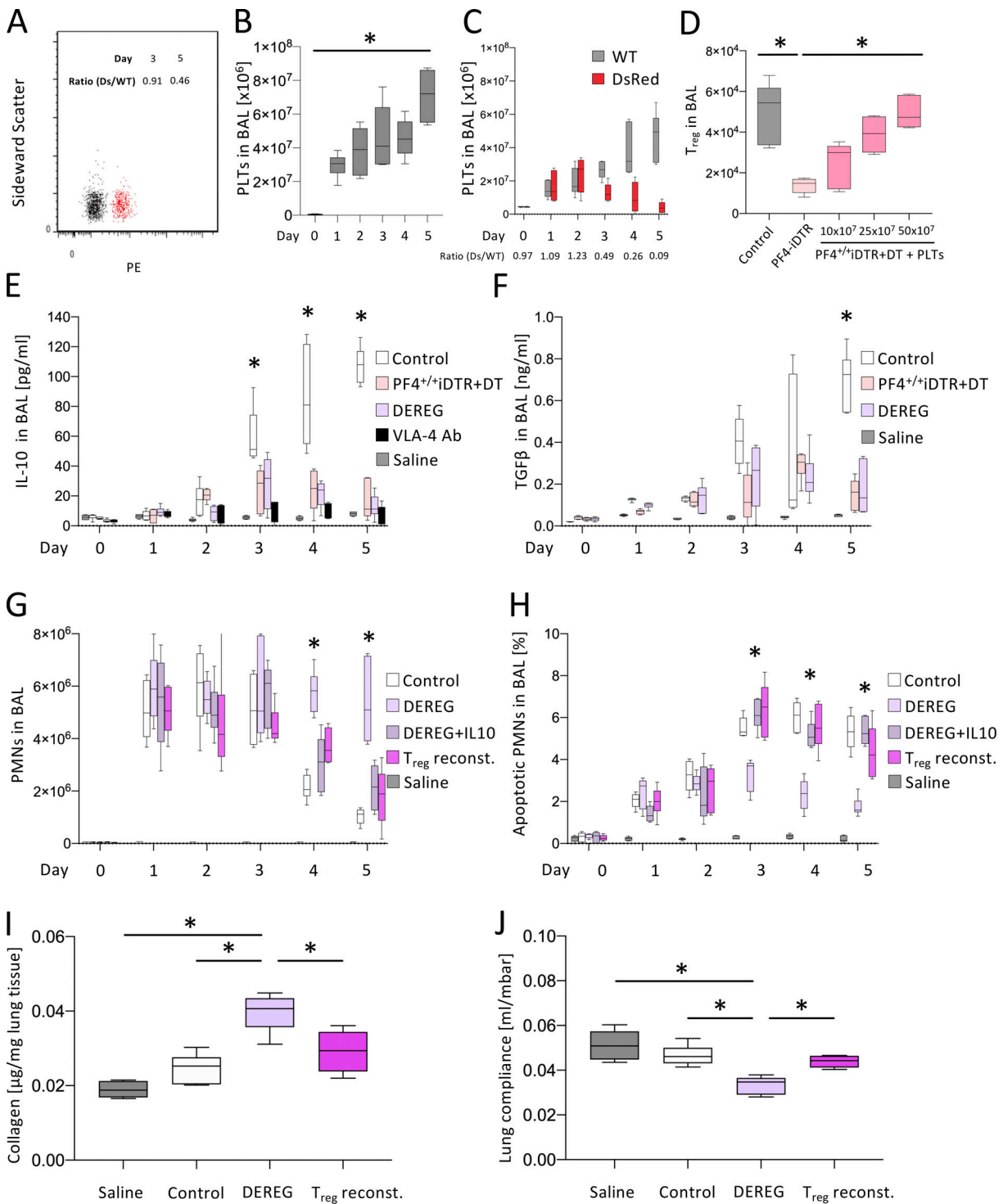


Figure 3. Platelets regulate IL-10 and TGFβ cytokine homeostasis and guide Treg cells to inflamed alveoli. (A) Bacterial pneumonia was induced in WT mice and red fluorescent platelets isolated from DsRed⁺ mice were injected at day 3 and detected in the BAL fluid by flow cytometry on day 5 (representative plot from two experiments with four to six mice in each group). Ratios of DsRed⁺:WT platelets are provided for days 3 and 5. (B) Bacterial pneumonia was induced in WT mice and platelets in the BAL fluid were analyzed by flow cytometry (data pooled from at least two independent experiments with four to six mice in each group; Mann-Whitney test was used for statistical analysis, *, P < 0.05). (C) Isolated DsRed⁺ platelets were injected into WT mice before induction of bacterial pneumonia and platelets in the BAL fluid were analyzed by flow cytometry. Ratios of DsRed⁺:WT platelets are provided each day (data pooled from three independent experiments with four to six mice in each group; Mann-Whitney test was used for statistical analysis, *, P < 0.05). (D) Bacterial pneumonia was induced in WT and PF4^{+/+}iDTR+DT mice (receiving DT) by i.t. instillation of viable *K. pneumoniae*. On day 3, platelet-depleted mice were reconstituted with isolated WT donor platelets by intravascular injection at different concentrations and recruitment of Treg cells in the BAL fluid was analyzed by flow cytometry on day 5. (E and F) Bacterial pneumonia was induced in WT, PF4^{+/+}iDTR+DT, and DERE mice by i.t. instillation of viable *K. pneumoniae* (1.5 × 10⁷ CFU/mouse) and the concentrations of the cytokines IL-10 (E) and TGFβ in the BAL (F) were analyzed by ELISA (data pooled from two independent experiments with four to

six mice in each group; Mann-Whitney test was used for statistical analysis, *, $P < 0.05$). Bacterial pneumonia was induced in DERE mice or DERE mice that were reconstituted with isolated WT donor T reg cells or recombinant IL-10 (200 ng/mouse i.t.) 2 d after induction of pneumonia. **(G and H)** The number of neutrophils in the BAL fluid (G) and the percentage of apoptotic neutrophils in the BAL (H) was analyzed by flow cytometry (data pooled from two independent experiments with four to six mice in each group; Mann-Whitney test was used for statistical analysis, *, $P < 0.05$). **(I and J)** 14 d after induction of pneumonia, lung collagen content (I) and lung compliance (J) were analyzed (data pooled from at least two independent experiments with four to six mice in each group; Mann-Whitney test was used for statistical analysis, *, $P < 0.05$). PLT, platelet.

L). In particular, genes coding for anti-inflammatory mediators (*Il10*, *Il13*, *Gdf15*), GTPase-activating proteins (*Arhgap25*, *Arhgap24*), and genes regulating terminal cell maturation (*Irf8*, *Ifi207*, *Pias1*) and activation (*Tspan31*, *Nfaml*) in T reg cells were significantly downregulated in the absence of platelets. These findings led to the hypothesis that platelets modulate and boost the anti-inflammatory and reparative properties of T reg cells and contribute to resolution of inflammation in the lungs.

Platelets are present in alveoli during recovery from pulmonary inflammation

Previous reports have shown the intra-alveolar presence of platelets during pulmonary inflammation (Ortiz-Muñoz et al., 2014). We performed electron microscopy and could indeed detect platelets within the lung alveoli (Fig. 5, A–F), which was in agreement with our flow cytometry analyses (Fig. S2 D). Platelet counts in the BAL increased 5 d following pneumonia induction (Fig. 5 G). To investigate which cell type afforded platelet relocation into the alveoli, we induced bacterial pneumonia in control mice and *Mrp8^{IDTR}* mice in which DT administration led to neutrophil depletion before pneumonia induction (Fig. S3 D). Neutrophil depletion significantly decreased the number of detectable platelets in the BAL after pneumonia induction (Fig. 5 G). In contrast, T reg cell depletion in DERE mice did not alter platelet relocation into the alveoli in the early stages of disease. Rather, reductions were seen at later times, which together indicated temporally restricted shuttling of platelets by each cell type, with T reg cells dominating at late times (Fig. 5 G). Consistent with the requirement of platelets for the immunomodulatory effect of T reg cells, we found that platelet depletion decreased TGFβ and IL-10 levels in the BAL (Fig. 5, H and I).

Finally, we visualized platelet relocation into the alveoli during pneumonia. We analyzed lung sections from mice 3 d (Fig. 5, J–L) and 5 d (Fig. 5, M–P) after pneumonia induction by confocal microscopy. By using confocal microscopy, we also detected platelet–T reg cell aggregates in the lung at day 5 after induction of pulmonary inflammation (Fig. 5 Q). Platelet accumulation in the alveolar space was significantly attenuated by prior neutrophil depletion in *Mrp8^{IDTR}* mice (Fig. 5 R). Platelet–neutrophil interactions in the lung tissue rose up by day 3, followed by a decrease on day 5 (Fig. 5 S). Together, these data demonstrate that platelets require neutrophils and T reg cells to relocate into the alveolar space at the onset and during the resolution of bacterial-induced inflammation.

Intra-alveolar platelets drive polarization toward resolving macrophages

Alveolar macrophages are among the first cells that detect bacterial infections and initiate an immune response (Kaur et al.,

2015). Increased macrophage numbers in the BAL were detectable until at least 4–5 d after pneumonia induction, but neither platelet nor T reg cell depletion modulated macrophage numbers (Fig. 6 A). To assess whether alveolar macrophages were recruited from the blood, we injected isolated eGFP⁺ monocytes in WT mice and observed the appearance of alveolar macrophages in the lung after pneumonia induction, confirming at least in part a blood origin (Fig. S5, A–C). To assess the functional role of macrophages in the resolution phase of bacterial-induced pulmonary inflammation, macrophages were depleted by injecting chlodronate liposomes. The efficiency of macrophage depletion in the lung alveolar and interstitial space was verified to be >95%. Macrophage depletion on day 2 after the induction of pulmonary inflammation significantly increased neutrophil counts in the BAL and interstitial compartment and decreased neutrophil apoptosis on the consecutive days to a level similar to platelet depletion on day 2 after induction of pneumonia. In fact, combined macrophage and platelet depletion did not show an additional effect (Fig. S5, D–G).

Macrophages have been shown to mediate the clearance of apoptotic neutrophils in alveoli (Fadok et al., 1998; Levy and Serhan, 2014). Consistently, we found that macrophages took up eGFP⁺ neutrophils in *LysM-Cre/eGFP* mice, confirming that dying neutrophils are phagocytosed by macrophages during the resolution phase (data not shown). The persisting intra-alveolar accumulation of neutrophils 5 d after pneumonia induction caused by platelet depletion on day 2 could be reversed by i.t. instillation of platelets in a concentration-dependent manner, but not by cell-free platelet supernatant or 50 μl ADP alone (10 μM; Fig. 6 B). Likewise, the amount of apoptotic neutrophils after platelet depletion was increased by instilled platelets (Fig. 6 C). As i.t. instillation would be challenging in the clinical context, we also transfused platelets i.v. in platelet-depleted mice and observed decreased intra-alveolar accumulation of neutrophils and an increased percentage of apoptotic neutrophils 5 d after inducing pneumonia (Fig. 6, B and C).

To investigate the role of platelets on differential transcriptome regulation, we induced pneumonia, depleted platelets after 3 d, and isolated pro- (CD68⁺CD80⁺) and anti-inflammatory (CD68⁺CD163⁺) macrophages from the BAL at day 5. RNA sequencing (RNaseq) analysis of pro-inflammatory macrophages revealed very few genes that were differentially expressed (DE; Fig. 6, D and G). Platelet depletion predominantly led to the upregulation of genes encoding for adenosin signaling (*Adora1*), apoptosis inhibition (*Faim2*), metabolism of GTP- and GDP-binding proteins (*Rab40c*), and inflammatory cell surface receptors (*Ptgfr*, *Il9r*). In contrast, platelet depletion led to the differential regulation of 811 genes in anti-inflammatory macrophages (Fig. 6, E and H), with differential downregulation of

ml), or thrombin (0.1 U/ml) in vitro. **(B and C)** Surface P-selectin expression (B) and platelet fibrinogen binding (C) were analyzed by flow cytometry (data pooled from at least two independent experiments with six samples in each group; Mann-Whitney test was used for statistical analysis). **(D)** Platelet shape change after sCD40L stimulation was analyzed by light microscopy (data pooled from three independent experiments with three samples in each group). Platelet spreading stages were identified as round (S1), filopodia formation (S2), filopodia and lamellipodia formation (S3), and fully spread (S4). Scale bar, 2 μ m. **(E)** Aggregometry in murine PRP was analyzed in unstimulated samples or after stimulation with sCD40L (20 ng/ml) or thrombin (0.1 or 1.0 U/ml; exemplary graphs from three independent experiments). Isolated WT T reg cells and platelets were cocubated in vitro in the presence or absence of blocking antibodies against P-selectin (clone RB40.34, 5 μ g/ml), PSGL-1 (clone 4RA10, 5 μ g/ml), or CD40 (clone HM40-3, 5 μ g/ml) and left unstimulated or stimulated with sCD40L (20 ng/ml) for 1 h at 37°C. **(F)** Platelet-T reg cell interactions were analyzed by flow cytometry. **(G and H)** The concentrations of the cytokines IL-10 (G) and TGF β (H) in the supernatant from the platelet-T reg cell cocultures were analyzed by ELISA (data pooled from at least two independent experiments with five samples in each group; Mann-Whitney test was used for statistical analysis, *, $P < 0.05$). Bacterial pneumonia was induced in WT mice and CD40L^{-/-} mice by i.t. instillation of viable *K. pneumoniae* (1.5×10^7 CFU/mouse). Some WT mice received Fab fragments of blocking antibodies against P-selectin (clone RB40.34, 50 μ g/mouse), CD40 (clone HM40-3, 50 μ g/mouse i.v.), or isotype control 2 d after induction of pneumonia. **(I and J)** The number of T reg cells (I) and neutrophils (J) in the BAL fluid was analyzed by flow cytometry (data pooled from at least two independent experiments with four to six mice in each group; Mann-Whitney test was used for statistical analysis, *, $P < 0.05$). To conduct RNaseq in the lung during resolution of pulmonary inflammation, single T reg cells, platelet-T reg cell aggregates, and macrophages were isolated from BAL fluid obtained at day 5 after induction of bacterial pneumonia from WT mice and platelet-depleted WT mice. **(K and L)** Heat map with hierarchical tree (K) and volcano plot (L) comparing differences of RNaseq-based gene expression values in T reg cells after physical binding to platelets.

genes governing inflammatory pathways (*Anxa11*, *Rapbp1*, *CD86*, *Pkn1*, *RhoC*) and upregulation of genes modulating cell differentiation (*Fgf1*). We could identify 61 genes in pro-inflammatory macrophages and 804 genes in anti-inflammatory macrophages that were differentially regulated following platelet depletion, and seven genes (*Faim2*, *Gm15758*, *Gm40649*, *Lgi1*, *Pfn4*, *Ssl81l*, *Synpr*) that were differentially regulated in the same direction in both macrophage populations after platelet depletion (Fig. 6 F). Gene ontology analysis revealed the significant regulation of nine distinct pathways, including the regulation and organization of nucleus, nucleolus, cytoplasm, protein-containing complex, trans-Golgi network, and genes regulating leukocyte apoptosis. In particular, the gene *Pfn4* has been linked to playing a role in cytoskeletal rearrangement and efferocytosis (Benoit et al., 2012; Wang et al., 2018), and the gene *Tspan3*, a member of the tetraspanin family of genes involved in the organization of the engulfment synapse (Barth et al., 2017), was downregulated on anti-inflammatory macrophages in the absence of platelets. This finding led us to the hypothesis that the presence of intra-alveolar platelets triggered neutrophil clearance by reprogramming macrophages. We isolated macrophages from BAL fluid obtained 5 d after pneumonia induction and analyzed gene expression. The pro-inflammatory phenotype was characterized by upregulated expression of *Gpr18* and *Fpr2*, whereas *EGR2* and *c-Myc* were characteristic of the anti-inflammatory phenotype (Jablonski et al., 2015). Macrophages isolated from platelet-depleted mice infected with *Klebsiella pneumoniae* showed a shift toward a pro-inflammatory polarization of macrophages, which could be reversed by injecting platelets i.t. into platelet-depleted animals (Fig. 6 I). A similar pro-inflammatory shift could be detected when isolated alveolar macrophages from untreated control mice were incubated with BAL fluid from platelet-depleted mice (Fig. 6 J). Furthermore, significantly higher levels of TNF α and IFN γ could be detected in the BAL supernatant in the absence of platelets (Fig. S5, H and I). These data indicate that platelets are crucially needed for the polarization and education of anti-inflammatory macrophages during resolution.

To test the phagocytic capability of macrophages to ingest isolated, ex vivo apoptotic neutrophils, we isolated alveolar

macrophages from control mice and platelet-depleted mice 5 d after pneumonia induction (Andonegui et al., 2003). The efferocytosis index of macrophages isolated from platelet-depleted mice was significantly lower than in macrophages from platelet-competent mice (Fig. 6 K). A similar effect on the efferocytosis index could be detected in isolated alveolar macrophages from untreated mice incubated with BAL fluid obtained from control mice and platelet-depleted mice 5 d after pneumonia induction (Fig. 6 L). Efferocytosis could be restored by i.t. instillation of isolated platelets into platelet-depleted mice (Fig. 6 L).

To further characterize macrophage polarization, we isolated macrophages at day 5 after pneumonia induction and detected an upregulation of anti-inflammatory genes (Jablonski et al., 2015), whereas intra-alveolar platelet depletion led to increased inflammation-associated gene expression (Fig. 7 A). Interestingly, *Gpr18* and *Fpr2*, both well-known receptors binding pro-resolving lipid mediators, were increasingly expressed on macrophages in platelet-depleted mice. Thus, we analyzed the expression profile of pro-resolving lipid mediators at day 5 after pneumonia induction in the lung tissue of mice that received a platelet-depleting or control antibody at day 2 after pneumonia induction. Platelet depletion significantly increased the levels of resolvin D4 (RvD4), resolvin E4 (RvE4), lipoxin A4 (LXA4), and 15-epi-LXA4, whereas the levels of resolvin D6 (RvD6), leukotriene B4 (LTB4), leukotriene C4 (LTC4), leukotriene D4 (LTD4), and leukotriene E4 (LTE4) were significantly decreased compared with isotype-treated mice (Fig. 7, B–D).

To investigate whether pro-resolving macrophage polarization is driven by direct cellular interactions with T reg cells and/or platelets, or by soluble mediators, we incubated isolated macrophages with T reg cells alone or with T reg cells and platelets, or with the supernatant taken from these cells. We observed resolving-type macrophage polarization after incubation with T reg cells and ADP- or thrombin-activated platelets, or with the supernatant from a coculture of both cells but not with T reg cells alone (Fig. 8, A and B). Consistent with these findings, efferocytosis significantly increased when isolated macrophages were incubated with T reg cells and ADP- or thrombin-activated platelets, or with their supernatant (Fig. 8, C and D).

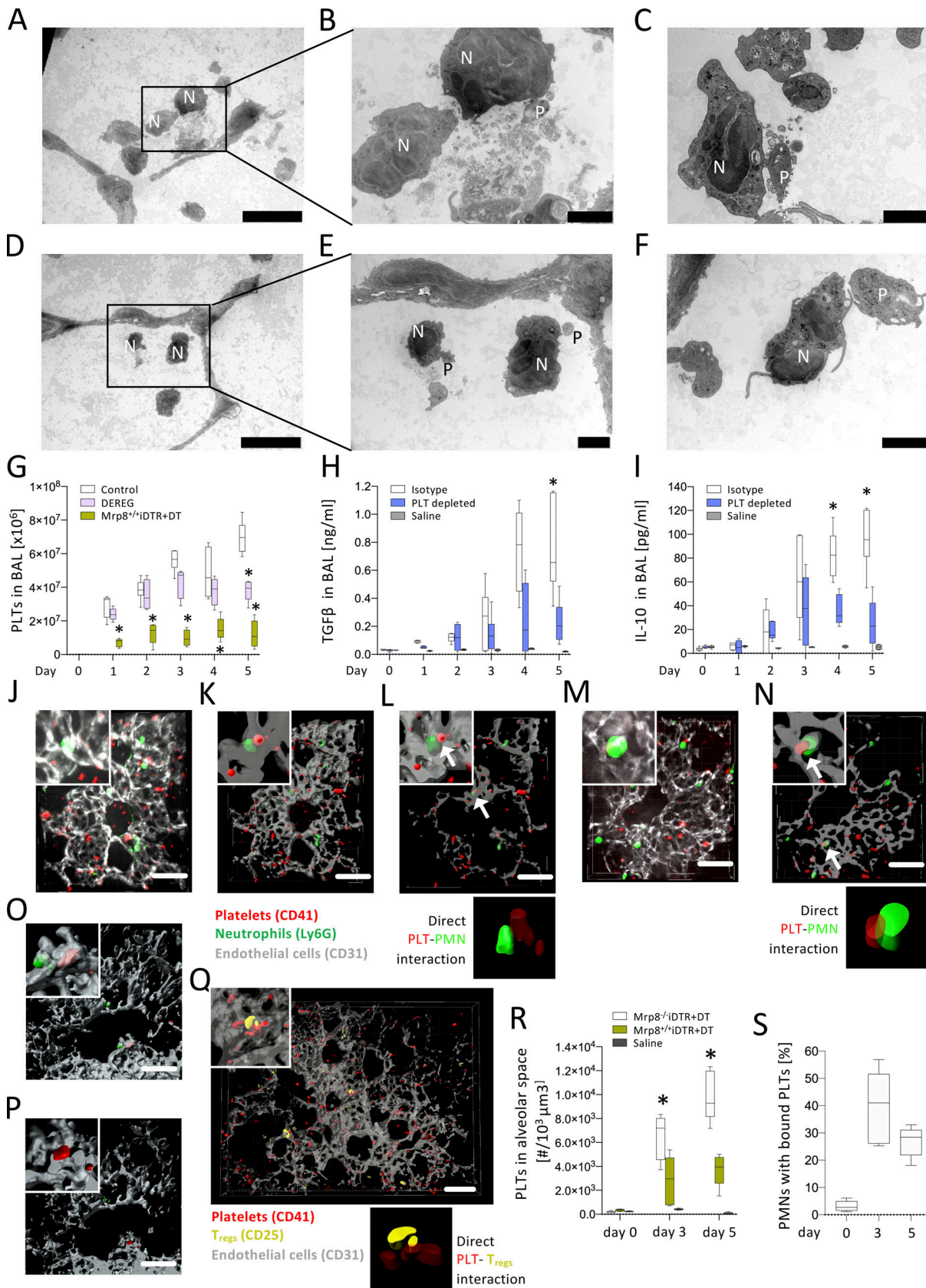


Figure 5. **Platelets are in alveoli during recovery from pulmonary inflammation.** Bacterial pneumonia was induced in WT mice. (A–F) Ultrathin cross-sectioned lung tissue imaged by transmission electron microscopy WT mice after inducing pneumonia showing neutrophils (N) in close proximity to platelets (P) within the lung intra-alveolar space. Bacterial pneumonia was induced in WT, DEREG, and Mrp8^{+/-}iDTR+DT (receiving DT) mice by i.t. instillation of viable K.

pneumoniae (1.5×10^7 CFUs/mouse; exemplary images from at least two independent experiments with three mice in each group, black scale bars in A and D equal 10 μm , scale bars in B, E, and F equal 2 μm , and scale bar in C equals 1 μm). **(G)** Platelet counts in the BAL in MRP8-iDTR and DERE mice. **(H and I)** Concentrations of the cytokines TGF β (H) and IL-10 (I) in the BAL fluid were analyzed by ELISA (data pooled from at least two independent experiments with four to six mice in each group; Mann-Whitney test was used for statistical analysis, *, $P < 0.05$). **(J–L)** Confocal image of lung tissue with terminal alveolae from WT mice (J) 3 d after induction of pneumonia with (K) 3D reconstruction and (L) exemplary display of a single confocal plane to identify neutrophils (Ly6G, green) and platelets (CD41, red) within pulmonary capillaries stained with PECAM-1 antibody (CD31, gray). Scale bar, 50 μm . Lower insert displays exemplary 3D reconstruction of direct interaction of platelets (CD41, red) and neutrophils (Ly6G, green). **(M and N)** Confocal image of lung tissue from WT mice (M) 5 d after induction of pneumonia with (N) exemplary display of a single confocal plane to identify neutrophils (Ly6G, green) and platelets (CD41, red) within pulmonary capillaries stained with PECAM-1 antibody (CD31, gray). Scale bar, 50 μm ; inserts with higher magnification in upper left corner and lower insert displays exemplary 3D reconstruction of direct interaction of platelets (CD41, red) and neutrophils (Ly6G, green). White arrows indicate sites of direct platelet–neutrophil interactions. **(O and P)** Confocal image of lung tissue from MRP8^{+/iDTR}+DT mice (O) 5 d after induction of pneumonia with (P) exemplary display of a single confocal plane to identify neutrophils (Ly6G, green) and platelets (CD41, red) within pulmonary capillaries stained with PECAM-1 antibody (CD31, gray). Scale bar, 50 μm ; inserts with higher magnification in upper left corner. **(Q)** Confocal image of lung tissue from WT mice 5 d after induction of pneumonia with exemplary display of a single confocal plane to identify T reg cell (CD25, yellow) and platelet (CD41, red) aggregates within the lung tissue. Scale bar, 50 μm ; lower insert displays exemplary 3D reconstruction of direct interaction of platelets (CD41, red) and T reg cells (CD25, yellow). Bacterial pneumonia was induced in WT and MRP8^{+/iDTR}+DT (receiving DT) mice (inserts with higher magnification in upper left corner). **(R and S)** Platelet accumulation in the alveolar space (R) and the quantification of platelet–neutrophil interactions (S) was analyzed by confocal image of lung tissue from WT mice 3 and 5 d after induction of pneumonia (exemplary images from at least three independent experiments with three mice in each group; Mann-Whitney test was used for statistical analysis, *, $P < 0.05$). PLT, platelet.

To gain mechanistic insights into the cellular crosstalk, we next cocultured T reg cells with or without activated platelets and/or macrophages and blocked protein de novo synthesis by actinomycin. We observed that IL-10 and TGF β were only produced by T reg cells in the presence of ADP- or thrombin-activated platelets (Fig. 9, A and B). These data indicate that the simultaneous presence of T reg cells and activated platelets is necessary to produce IL-10 and TGF β de novo, which, in turn, mediate the polarization of macrophages toward a pro-resolving phenotype. These data indicate that T reg cells respond transcriptionally to platelet binding.

Finally, to further analyze the source of IL-10 and TGF β , we analyzed *Il10* and *Tgfb1* mRNA expression in isolated T reg cells and macrophages and observed a higher expression in T reg cells (Fig. 9 C). Blocking both cytokines led to persistently higher neutrophil counts and decreased neutrophil apoptosis in the BAL (Fig. 9, D and E). In contrast, the numbers of T reg cells and platelets in the BAL were not affected by IL-10 and TGF β blockade (Fig. 9, F and G), altogether demonstrating that T reg cell–platelet coupling elicits the anti-inflammatory, pro-resolving fate of alveolar macrophages to terminate inflammation and protect the host.

Discussion

Neutrophil apoptosis and macrophage education is the major route to clear neutrophils and maintain homeostasis (Bratton and Henson, 2011). Macrophage phagocytosis not only prevents secondary necrosis of apoptotic neutrophils and neutrophil debris and pro-inflammatory signal release, but also polarizes macrophages toward an anti-inflammatory phenotype (Kennedy and DeLeo, 2009). Here, we demonstrate that platelets, which have been involved in the onset of inflammation, are equally important in the resolution phase by mediating T reg cell recruitment into the alveoli, a process that is dependent on CD40–CD40L and P-selectin/PSGL-1 interactions. Furthermore, platelets and T reg cells cooperate in the resolution process by orchestrating macrophage polarization toward a reparative phenotype and increase the efferocytosis

capacity of macrophages in the alveoli needed for the clearance of residual neutrophils.

Several studies have provided evidence that platelets appear in the lung alveoli (Pitchford et al., 2008; Zarbock et al., 2006). Furthermore, platelets eventually coupled to leukocytes can be detected in the BAL after induction of pulmonary inflammation (Amison et al., 2018; Lax et al., 2017; Ortiz-Muñoz et al., 2014). This is well in accordance with our findings that platelets translocate into the alveoli during the inflammatory phase and during the resolution process following pulmonary inflammation. Our study demonstrates for the first time that platelets get recruited to the lung during the onset of resolution, together with T reg cells. Platelets were long thought to be passive blood cells reaching their site of action by chance, enforced by their sheer numbers (Herter et al., 2014). Contradicting this dogma, platelets are now known to be capable of active migration (Gaertner et al., 2017). Interestingly, platelet recruitment into the lung vasculature and tissue does not entirely rely on the distinct mechanisms that mediate pulmonary neutrophil accumulation together with platelets but also appear to exist independently (Cleary et al., 2019). This fits well with our observation that the distribution of platelets is not only restricted to the intravascular compartment, but that platelets also translocate toward the alveoli.

Previous studies have suggested that platelets may not only be important for the propagation of vascular inflammation—for example, platelet-activating factor plays a role in mediating urate crystal uptake during the resolution of gouty inflammation (Yagnik, 2014). Platelets are also a major source for anti-inflammatory mediators of the lipoxin family (e.g., specialized pro-resolving mediators, such as resolvins, protectins, and maresins; Yadav and Kor, 2015). These lipoxins are produced and released already during the inflammatory onset phase of acute inflammation, and their concentrations sharply rise during the convergence toward the resolution phase (Haworth et al., 2008). Interestingly, these lipoxins also promote phagocytic clearance of apoptotic immune cells during resolution (Mitchell et al., 2002). This evidence aligns with our observations that platelets and T reg cells in the alveoli are needed

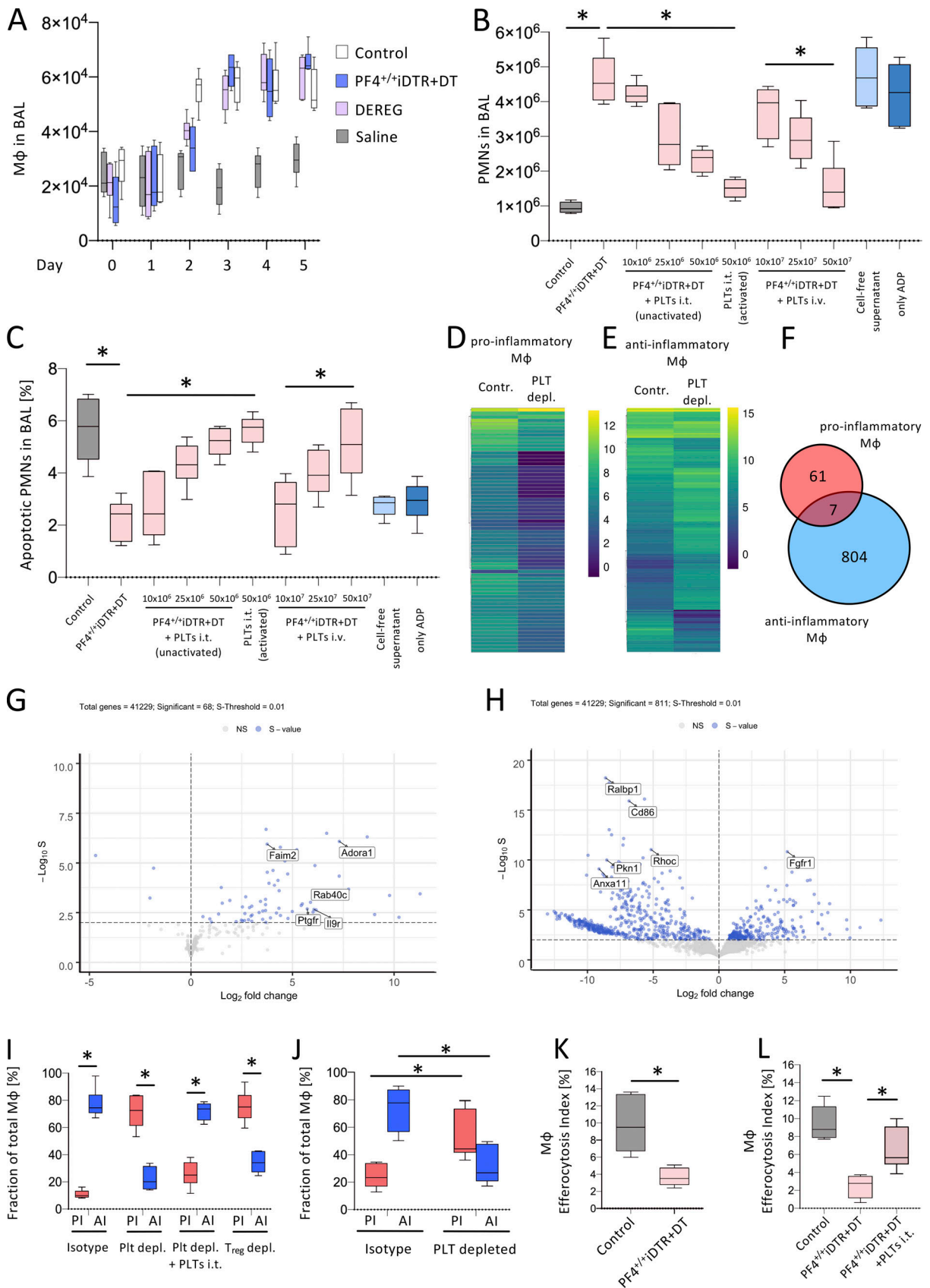


Figure 6. **Intra-alveolar platelets drive polarization toward resolving macrophages.** Bacterial pneumonia was induced in WT, PF4^{+/+}iDTR+DT (receiving DT), and DEREK mice by i.t. instillation of viable *K. pneumoniae* (1.5 × 10⁷ CFUs/mouse). **(A)** The total number of macrophages (Mφ) in the BAL fluid was analyzed by flow cytometry (data pooled from at least two independent experiments with 5–6 mice in each group; Mann-Whitney test was used for statistical

analysis, *, $P < 0.05$). Pneumonia was induced in WT mice and PF4^{+/+}iDTR+DT (receiving DT) mice. Mice were i.t. or i.v. reconstituted with the indicated number of nonactivated or ADP-activated (10 μ m ADP) isolated WT donor platelets. **(B and C)** The number of neutrophils in the BAL fluid (B) and the percentage of apoptotic neutrophils in the BAL (C) were analyzed by flow cytometry (data pooled from two independent experiments with four to six mice in each group; Mann-Whitney test was used for statistical analysis, *, $P < 0.05$). To conduct RNaseq analysis of macrophages in the lung during resolution of pulmonary inflammation, pro- and anti-inflammatory macrophages were isolated from BAL fluid obtained at day 5 after induction of bacterial pneumonia from WT mice and platelet-depleted WT mice. **(D and E)** Heat map with hierarchical tree comparing differences of gene expression values induced by platelet depletion in (D) pro-inflammatory macrophages and (E) anti-inflammatory macrophages. Each line in heat map represents the changes in a given transcript. Yellow and blue colors represent increased and decreased gene expression, respectively. **(F)** Venn diagram of DE genes filtered by s -value < 0.01 in either pro-inflammatory and/or anti-inflammatory macrophages after platelet depletion. **(G and H)** Volcano plots comparing differences of gene expression values induced by platelet depletion in (G) pro-inflammatory macrophages and (H) anti-inflammatory macrophages (data pooled from three independent experiments with three mice in each group). Pneumonia was induced in control mice, in mice in which intravascular platelets were depleted by i.v. injection of a platelet-depleting antibody (clone R300, 2 μ g/g bodyweight) 2 d after induction of pneumonia, and in mice that were i.t. reconstituted with unactivated or activated WT donor platelets. **(I)** Macrophage polarization in the BAL fluid obtained 5 d after induction of pneumonia was analyzed by qRT-PCR (data pooled from three independent experiments with 5–6 mice in each group; Mann-Whitney test was used for statistical analysis, *, $P < 0.05$). **(J)** Isolated alveolar macrophages from untreated WT mice were incubated with BAL fluid obtained from control mice and platelet-depleted mice 5 d after induction of pneumonia and macrophage polarization was analyzed by qRT-PCR (data pooled from three independent experiments with 5–6 mice in each group; Mann-Whitney test was used for statistical analysis, *, $P < 0.05$). **(K)** Efferocytosis index of macrophages obtained from control mice and PF4^{+/+}iDTR+DT (receiving DT) mice 5 d after induction of pneumonia (data pooled from three independent experiments with 5–6 mice in each group; Mann-Whitney test was used for statistical analysis, *, $P < 0.05$). **(L)** Efferocytosis index of isolated alveolar macrophages from untreated mice incubated with BAL fluid obtained from control mice and PF4^{+/+}iDTR+DT (receiving DT) mice 5 d after induction of pneumonia (data pooled from three independent experiments with 5–6 mice in each group; Mann-Whitney test was used for statistical analysis, *, $P < 0.05$). AI, anti-inflammatory; PI, pro-inflammatory.

to induce a shift toward the anti-inflammatory macrophage phenotype to support the clearance of inflammatory immune cells and resolution. Interestingly, expression of two major receptors (Gpr18 and Fpr2) for pro-resolving lipid mediators was found to be increased on macrophages in the presence of platelets. Likewise, major resolvins-class lipid mediators were found to be increased on day 5 in platelet-depleted animals in which resolution appeared to be impaired. One possible explanation for this finding may be an as-yet-unknown feedback mechanism that leads to a prolonged anti-inflammatory lipid mediator profile in the lung to compensate for the loss of the pro-resolving action of platelets during this stage. Furthermore, it is also possible that these particular mediators are not involved in the resolution process. However, it has to be acknowledged that the analysis of lipid pro- and anti-inflammatory mediators on day 5 in this study only represents a snapshot and warrants further experiments to better characterize the underlying molecular mechanisms in more detail.

Platelets have been previously described to interact with T reg cells under inflammatory conditions. It was shown that platelets are needed to control the anti-inflammatory actions of CD4⁺ T reg cells following burn injury (Bergmann et al., 2016). These findings are in accordance with ours, including the time periods (2–7 d) after which platelets regulate T reg cell-mediated responses. Beyond the lungs, platelets have also been shown to interact with CD4⁺ T cells in the liver following ischemic injury and during atherosclerosis (Khandoga et al., 2006; Li et al., 2013). Moreover, the CD40/CD40L axis is crucial for the interplay between platelets and T reg cells in atherosclerosis (Lievens et al., 2010). These findings again agree with the observations made here showing that platelet P-selectin, PSGL-1 on T reg cells, and the CD40/CD40L axis are needed for platelet–T reg cell complex formation as well as recruitment of these cells into the alveolar space during the resolution phase. We observed a time-dependent transition in platelet binding from neutrophils to T reg cells. We show that initial platelet binding to neutrophils appears to be diminished over time by decreasing surface

expression of PSGL-1, a phenomenon mediated by the sheddase ADAM8, leading to decreased neutrophil–platelet complex formation, as reported previously (Davenpeck et al., 2000; Domínguez-Luis et al., 2011). Mirroring the response in neutrophils, T reg cells upregulate PSGL-1 on the cell surface during the resolution phase that enables physical complexing with platelets. In this regard, it is interesting that platelets are thought to be capable of inducing CD4⁺ T cell differentiation by both the release of distinct cytokines and by direct cell–cell contact with T cells increasing IL-10 production and release by T cells (Gerdes et al., 2011). Indeed, we observed that the interaction of platelets and T reg cells is necessary for cytokine production (IL-10 and TGF β) by T reg cells, and that these are the mediators that induce macrophage polarization to enforce alveolar immune cell clearance.

It has recently become apparent that innate immune cells are constantly being reprogrammed in order to adjust their phenotypic behavior to the environmental needs (Adrover et al., 2020). While this concept is relatively new to neutrophils and T reg cells, macrophage reprogramming in response to various inflammatory or tissue conditions has long been known (Michaeloudes et al., 2020). This is the first study to demonstrate that direct platelet–T reg cell interactions modulate the T reg cell transcriptome, induce the secretion of cytokines that, in turn, reprogram macrophages for resolution. Further, we observed differential regulation of genes modulating efferocytosis only in anti-inflammatory macrophages, a finding in line with previously reports (Benoit et al., 2012; Wang et al., 2018).

T reg cell differentiation and turnover is critically dependent on dendritic cells (DCs). It has been shown that the suppression of the T reg cell/IL-10 axis of lung injury is DC dependent (Kapur et al., 2017a), yet the role of DCs on the regulation of the platelet–T reg cell interplay during the resolution of pulmonary inflammation remains unknown and warrants further research.

In summary, we have shown that platelets are recruited to the pulmonary alveoli and are actively involved in resolving

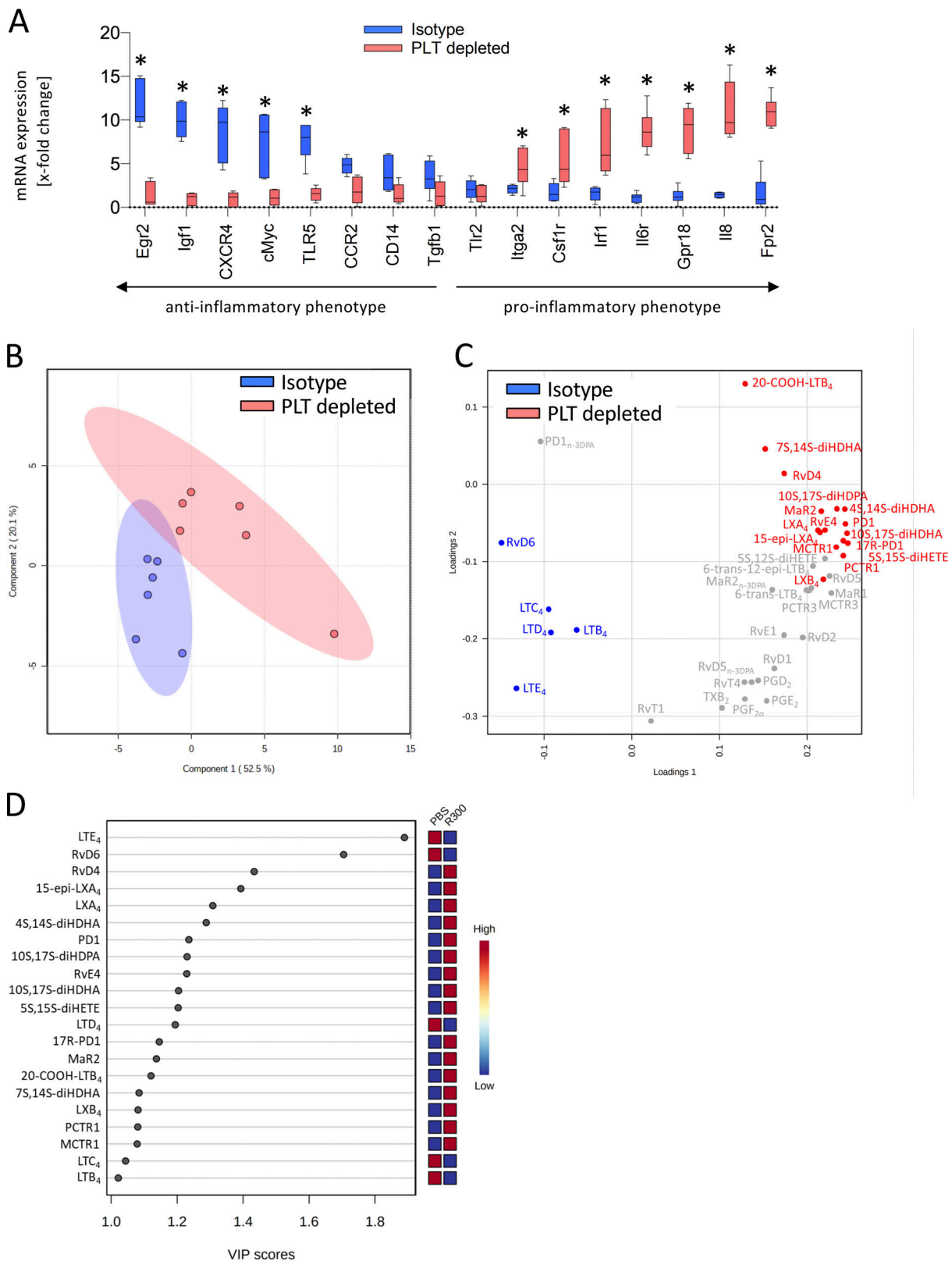


Figure 7. **Platelet depletion drives macrophage polarization and modulates pro-resolving lipid mediator balance in the lung.** Bacterial pneumonia was induced in WT mice by i.t. instillation of viable *K. pneumoniae* (1.5×10^7 CFUs/mouse). Mice received a platelet-depleting antibody (clone R300, 2 μ g/g body weight) or isotype control 2 d after induction of pneumonia. **(A)** Gene expression in isolated alveolar macrophages was analyzed by qRT-PCT 5 d after induction of pneumonia (data pooled from at least two independent experiments with four to five mice in each group; Mann-Whitney test was used for statistical analysis, *, $P < 0.05$). Lungs from isotype-treated and platelet-depleted mice were flushed with PBS and harvested on day 5 after pneumonia induction and

pro-resolving lipid mediators in the lungs tissue were analyzed by liquid chromatography-mass spectrometry. (B-D) 2D score plot (B), loading plot (C), and variable importance (D) in projection score of mice lungs infected with *K. pneumonia* and injected with/without a platelet-depleting antibody (data pooled from two independent experiments with six mice in each group, *, $P < 0.05$).

inflammation, together with T reg cells. This interaction triggers a phenotypic macrophage shift toward a reparative phenotype and prevents excessive pulmonary injury after an infection. These findings are of clinical importance, as antiplatelet drugs are common in the clinic. Thus, a deeper understanding of the role of platelets in these situations may provide new opportunities to develop and adapt new treatment strategies to improve patient outcomes after pulmonary infectious and inflammatory diseases.

Materials and methods

Animals and reagents

We used 8–12-wk-old male C57BL/6 mice. Mice were kept in a barrier facility under specific pathogen-free conditions. Unless otherwise stated, all reagents were obtained from Sigma-Aldrich. We used Pf4^{iDTR}, Mrp8^{iDTR}, and DEREG mice on a C57BL/6 background to deplete platelets, neutrophils, or T reg cells, respectively, by administration of 400 ng DT, as previously described (Buch et al., 2005; Lahl and Sparwasser, 2011;

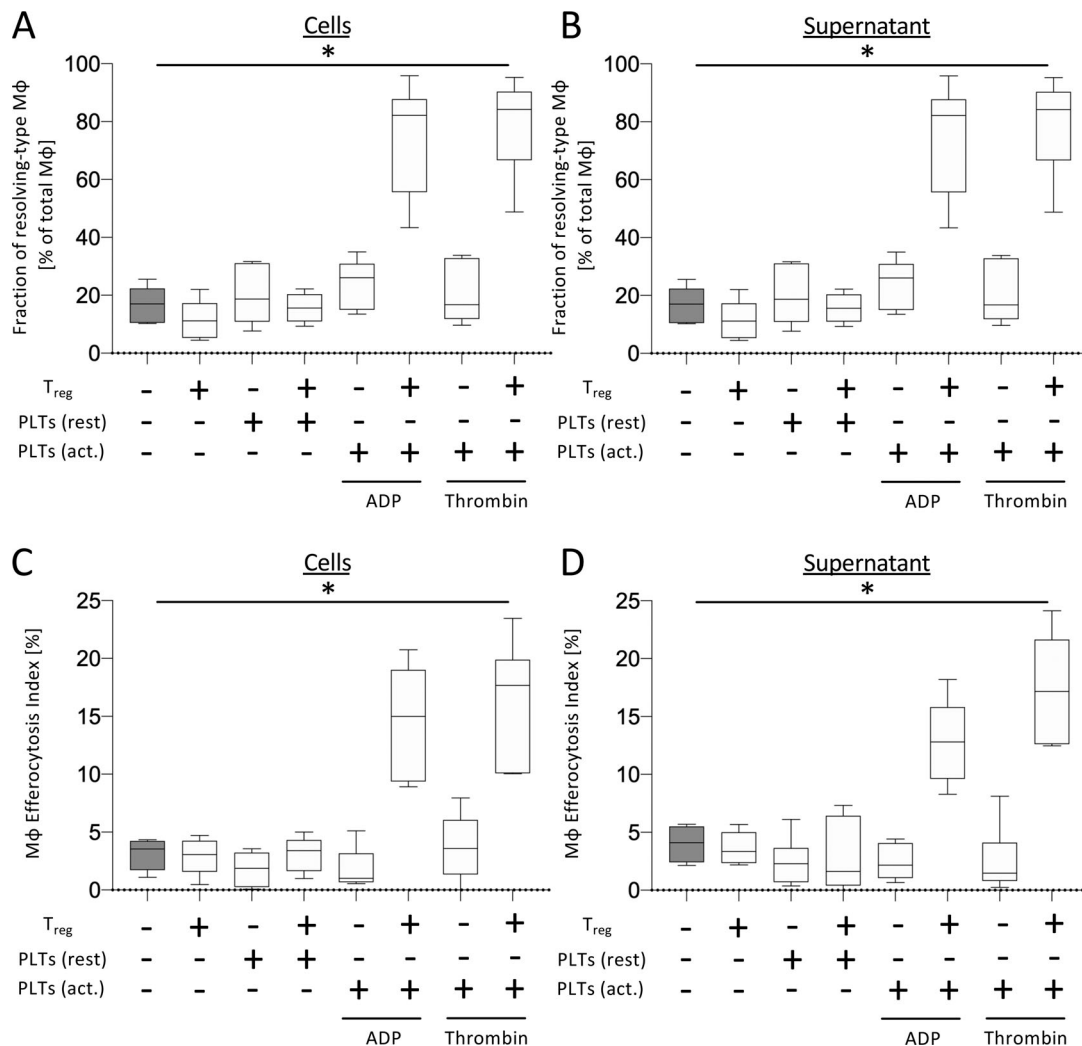


Figure 8. **Platelets and T reg cells drive macrophage polarization.** (A and B) Isolated alveolar macrophages from untreated WT mice were incubated with (A) T reg cells alone or in combination with resting, ADP (10 μ M)-, or human thrombin (0.1U ml⁻¹)-activated platelets; or (B) the supernatant from cocultures of T reg cells alone or in combination with resting, ADP-, or thrombin-activated platelets and macrophage polarization was analyzed by qRT-PCR (pooled data from three independent experiments with five samples in each group; Mann-Whitney test was used for statistical analysis, *, $P < 0.05$). (C and D) Isolated alveolar macrophages from untreated WT mice were incubated with (C) T reg cells alone or in combination with resting, ADP (10 μ M)-, or human thrombin (0.1U ml⁻¹)-activated platelets; or (D) the supernatant from cocultures of T reg cells alone or in combination with resting or ADP-activated platelets and the index of neutrophil efferocytosis was analyzed (pooled data from three independent experiments with five samples in each group; Mann-Whitney test was used for statistical analysis, *, $P < 0.05$).

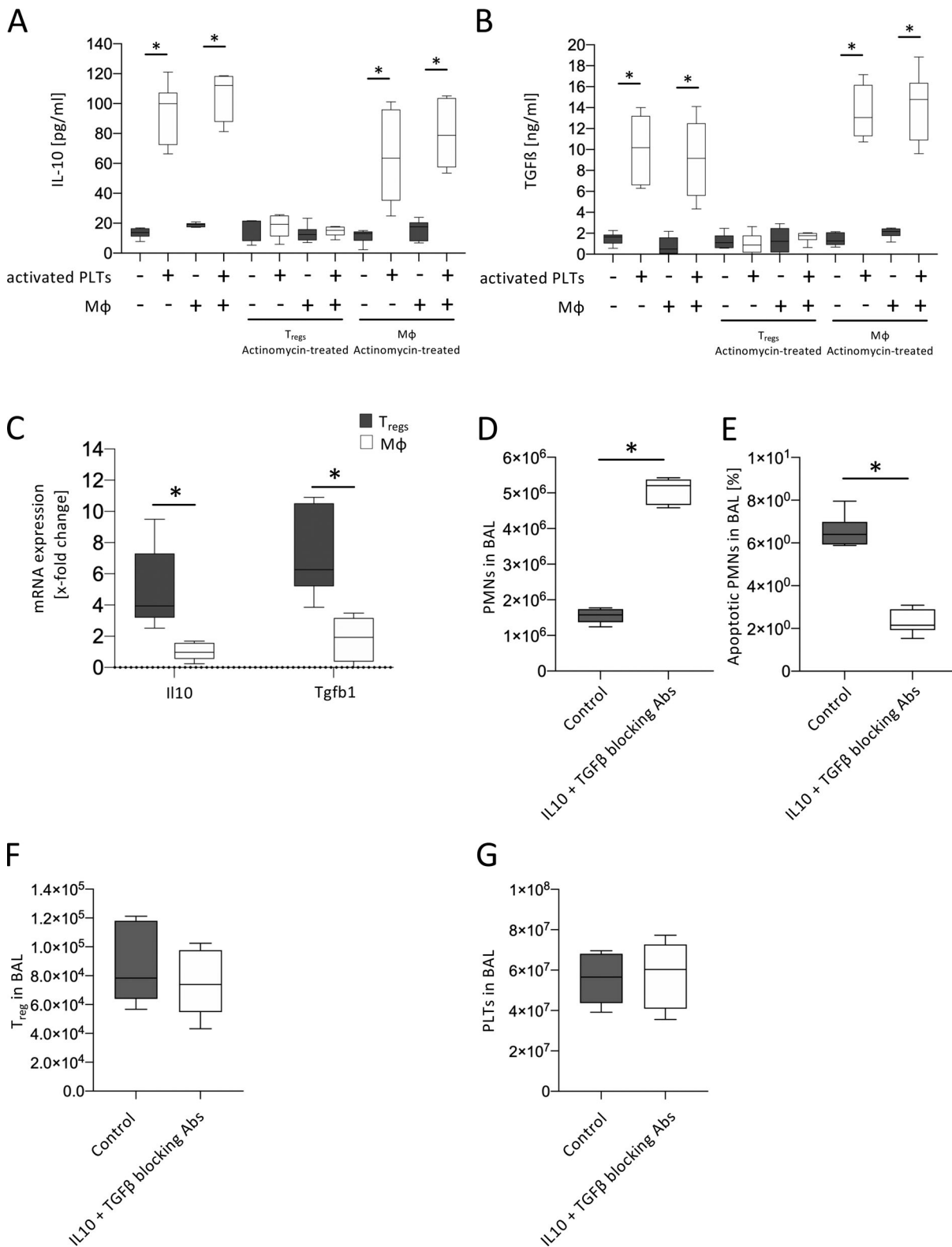


Figure 9. T reg cell-derived IL-10 and TGFβ mediate resolution of bacterial pneumonia. (A and B) Isolated T reg cells were coincubated with ADP-activated platelets and/or isolated macrophages and the concentration of (A) IL-10 and (B) TGFβ in the supernatant was analyzed (pooled data from three independent experiments with six samples in each group; Mann-Whitney test was used for statistical analysis, *, P < 0.05). Bacterial pneumonia was induced in WT mice by i.t. instillation of viable *K. pneumoniae* (1.5 × 10⁷ CFUs/mouse). **(C)** mRNA expression of IL10 and Tgfb1 in isolated alveolar macrophages and T reg cells was analyzed by qRT-PCT 5 d after induction of pneumonia. Mice received blocking antibodies against IL-10 (clone JES5-2A5, 50 μg/mouse) and TGFβ (clone 2G7, 100 μg/mouse) or isotype control 2 d after induction of pneumonia. **(D–G)** The number of (D) neutrophils in the BAL fluid, (E) the percentage of apoptotic neutrophils in the BAL, and the number of (F) T reg cells and (G) platelets was analyzed by flow cytometry (data pooled from two independent experiments with four mice in each group; Mann-Whitney test was used for statistical analysis, *, P < 0.05).

Wuescher et al., 2015). If not indicated otherwise, littermates were used as controls. All animal experiments were approved by the animal research committee of the Landesamt für Natur, Umwelt und Verbraucherschutz.

Murine pneumonia models

We used a murine pneumonia model as published by Ittner et al. (2012), with some modifications. Overnight cultures (37°C) of *K. pneumoniae* (strain 13883; American Type Culture Collection) were grown in tryptic soy medium, washed, and resuspended in sterile saline (0.9%). Mice were anaesthetized by intraperitoneal injection of ketamine (125 µg·g⁻¹ body weight; Pfizer) and xylazine (12.5 µg·g⁻¹ body weight; Bayer). Animals were challenged with 1.5×10^7 viable *K. pneumoniae* per mouse. At this inoculation dose, all mice survived the observation period. After the indicated time points, mice were sacrificed and the lungs were lavaged five times with 0.7 ml physiological saline solution. The number of leukocytes in the BAL was counted using kimura staining with an improved Neubauer counting chamber and an inverted cell culture microscope (Primovert; Carl Zeiss) equipped with a 10×/0.75 NA objective. A total of four fields with 16 standardized subfields in each individual field were counted for each sample. CFUs in the lung, blood, and spleen were counted by serial plating on tryptic soy agar plates (Ittner et al., 2012).

Analysis of viable lung sections ex vivo

Analysis of viable lung sections was performed as described before (Hasenberg et al., 2011). Mice were injected i.t. with *K. pneumoniae*. After 4 h, animals were injected with Alexa Fluor 488-coupled anti-Gr1 antibody (clone RB5-8C6; 5 µg/mouse, purified from hybridoma supernatant), Alexa Fluor 568-coupled anti-PECAM antibody (clone 390; 50 µg/mouse; BD Biosciences), and BV421-coupled anti-CD41 antibody (clone MWR30; 5 µg/mouse; BioLegend) to stain neutrophils, endothelial cells, and platelets. Mice were sacrificed and lungs were filled with 1 ml of low-melting agarose. After removal, lungs were cut using a vibratome. Lungs were fixed in a cell culture dish and submersed in PBS and z-stacks were recorded using a spinning disc confocal microscope (CellObserver SD; Carl Zeiss) equipped with a 20×/1.0 NA objective.

Efferocytosis assay

Approximately 10^5 isolated macrophages were seeded in a 24-well plate. Macrophages were incubated with 5-chloromethylfluorescein diacetate (CMFDA)-labeled neutrophils at a ratio of 1:1 and incubated at 37°C for 1 h. Excessive extracellular fluorescence was quenched with Trypan blue (0.04% in PBS). The proportion of macrophages (CD11b⁺F4/80⁺) with increased CMFDA fluorescence (indicating uptake of fluorescent-labeled apoptotic cells) was analyzed by flow cytometry on a FACSCantoII (BD Biosciences). The efferocytosis index was calculated as the percentage of macrophages showing increased CMFDA fluorescence as an indicator of neutrophil ingestion.

Leukocyte subset analysis by flow cytometry

Apoptotic neutrophils in the BAL fluid were analyzed by flow cytometry on a FACSCantoII (BD Biosystems) using an Annexin V staining. Macrophages in the BAL were analyzed by flow

cytometry by an F4/80 antibody, and T reg cells were identified based on their expression of CD4/CD25/FoxP3. Specific neutrophil accumulation in the intravascular, interstitial, and alveolar compartment was analyzed by a flow cytometry-based technique as described before (Reutershan et al., 2005). Neutrophils were depleted in some mice by injection of anti-Ly6G antibody (clone 1A8, 200 µg/mouse i.p.; BioLegend). Platelets were depleted in some mice by i.v. injection of a platelet-depleting antibody (clone R300; 2 µg/g bodyweight; Emfret). T reg cells were depleted in some mice by i.v. injection of an α-CD25 antibody (clone PC61; BioLegend; Setiady et al., 2010). Some mice were injected with blocking antibodies against P-selectin (clone RB40.34; 50 µg/mouse, purified from hybridoma supernatant) or CD40 (clone HM40-3; 50 µg/mouse; BioLegend).

Analysis of neutrophil recruitment into the intravascular, interstitial, and intra-alveolar space

Recruitment of neutrophils into the intravascular and interstitial compartment of the lung was determined as described previously (Zarbock et al., 2006). Briefly, Alexa Fluor 633-labeled Gr1 antibody (clone RB6-8C5, staining kit; Invitrogen) to murine neutrophils was injected i.v. 5 min before euthanasia. This procedure labels only intravascular neutrophils, as the time period is not sufficient for the antibody to react with neutrophils located in the interstitial or intra-alveolar compartment. Thoracotomy was performed, the inferior vena cava was opened, and nonadherent neutrophils were removed from the pulmonary vasculature by perfusing the right ventricle with 3 ml of saline with a constant pressure of 25 cmH₂O. After collection of the BAL, lungs were removed, minced, and digested with an enzyme cocktail (collagenase type XI, hyaluronidase type I-s, DNase1; Sigma-Aldrich) containing 65 µg of unlabeled Gr1 antibody at 37°C for 60 min. A cell suspension was made by passing the digested lung tissue through a 70-µm cell strainer (BD Falcon). RBCs were lysed and the remaining leukocytes were resuspended in PBS and counted. The fraction of neutrophils in the suspension was determined by flow cytometry (FacsCantoII; BD Biosciences). Neutrophils were identified by their typical appearance in the forward/side scatter and their expression of CD45 (clone 30-F11), 7/4 (clone 7/4; both BD PharMingen), and Gr1 (clone RB6-8C5, purified from hybridoma supernatant). The labeled Gr1 antibody was used to differentiate between intravascular (CD45⁺7/4⁺Gr1⁺) and interstitial (CD45⁺7/4⁺Gr1⁻) neutrophils.

Collagen content

To quantify the collagen content in the lung (as a measure for pulmonary fibrosis), the right lung lobes were excised, weighted, and homogenized. The tissue was hydrolyzed by addition of 12 N HCL and incubation at 120°C for 3 h. Samples were subsequently incubated with 4-dimethylaminobenzaldehyde for 90 min at 60°C. The absorbance of oxidized hydroxyproline was analyzed at 560 nm using a photometer.

Lung compliance

For the measurement of lung compliance, an endotracheal tube was placed by tracheotomy and connected to a precision syringe

connected to a pressure gauge. Static lung compliance was assessed by measuring the required inspiratory pressure to inflate the lung by an inspiratory volume of 1 ml room air and lung compliance was calculated (in mbar/ml).

Quantification of platelet–leukocyte interactions in vivo

Whole blood samples were withdrawn from mice and stained with Alexa Fluor 633–coupled anti-Gr1 antibody (clone RB6-8C5, purified from hybridoma supernatant), PE-coupled anti-CD41 antibody (clone MWRReg30; BD Biosciences), FITC-coupled anti-Ly6B2 antibody (clone 7/4; AbD Serotec), and PerCP-coupled anti-CD45 antibody (clone 30-F11; BD Biosciences). Platelet–neutrophil aggregates were quantified by measuring the percentage of CD41⁺ neutrophils (CD45⁺Gr1⁺7/4⁺) using a flow cytometer (BD FACSCantoII; BD Biosciences). To analyze aggregates of platelets and T reg cells, whole blood samples were stained with Alexa Fluor 633–coupled anti-CD4 antibody (clone GK1.5; BioLegend), PE-coupled anti-CD41 antibody (clone MWRReg30; BD Biosciences), FITC-coupled anti-CD25 antibody (clone PC61; BioLegend), and PerCP-coupled anti-CD45 antibody (clone 30-F11; BD Biosciences). Platelet–T reg cell aggregates were quantified using a flow cytometer (BD FACSCantoII; BD Biosciences).

Measurement of cytokine levels

Serum and coculture supernatant levels of IL-10, TGF β , and CD40 ligand were analyzed by commercially available ELISA sets following the manufacturer’s instructions (R&D Systems).

Alveolar macrophage isolation

Macrophages were isolated from BAL as described ([Andonegui et al., 2003](#)), adherence purified, and cultured in RPMI supplemented with 10% FCS, 1% penicillin, streptomycin, and fungizone.

Mouse neutrophil isolation

Femurs and tibias of mice were dissected, and the marrow was flushed with PBS and layered on a three-step Percoll gradient (72%, 64%, and 52%) and centrifuged at 1,060 $\times g$ for 30 min.

Platelet isolation

Citrate-anticoagulated whole blood samples were withdrawn from donor mice. Platelet-rich plasma (PRP) was separated by from whole blood by repetitive slow-speed centrifugation at 68 $\times g$ for 8 min. Platelets were isolated from PRP by centrifugation at 1088 $\times g$ for 5 min. Washed platelets were resuspended in Tyrode’s buffer and kept at 37°C before use. Platelet purity after isolation was >97%. Before i.t. injection, some platelets were stimulated with 10 μM ADP and injected i.t. in 50 μl Tyrode’s buffer.

T reg cell isolation

T reg cells were isolated from single-cell suspensions of the mouse spleen by using the CD4⁺CD25⁺ Regulatory T Cell Isolation Kit (Miltenyi Biotec).

Transmission electron microscopy

For electron microscopy, the lung was perfused with PBS via the right ventricle, followed by 2% glutaraldehyde, 2% paraformaldehyde

in 0.2 M cacodylate buffer (pH 7.4). The lung was removed and small samples were further fixed under low vacuum until they settled down on the bottom. The specimen was postfixed with 1% osmiumtetroxide and 1.5% potassium ferrocyanide, dehydrated, and embedded in epon. 60-nm ultrathin sections were cut (Leica UC6 ultramicrotome) and counterstained with uranyl acetate and lead. Samples were inspected on a transmission electron microscope at 80 kV (Fei-TecnaI2; FEI) and pictured with a CCD camera (Megaview; SIS).

Characterization of macrophage gene expression

BAL fluid was obtained from mice 5 d after induction of pneumonia by flushing the lungs with 5 \times ice-cold PBS/0.6 mM EDTA (Mg and Ca free). After centrifugation (450 $\times g$, 10 min), cells were resuspended in RPMI and allowed to adhere to the bottom of plastic 6-well plates during cultivation at 37°C/5% CO₂ for 45 min. Adherent macrophages were harvested after removal of supernatant. After RNA extraction using Trizol reagent and cDNA transcription (cDNA synthesis kit; Sigma-Aldrich), gene expression was analyzed by quantitative real-time PCR (qRT-PCR) using SYBR Green Mastermix (Life Technologies) on an Applied Biosystems 7600 Real-Time PCR device. The primer sequences were as follows: Gpr18: forward, 5’-GACAGACAGGAG GTTCGACATACA-3’; reverse, 3’-TGTATTCTCTGGGTGGAG CCA-5’; Fpr2: forward, 5’-TCTACCATCTCCAGAGTTCTGTGG-3’; reverse, 5’-TTACATCTACCACAATGTGAACTA-3’; Egr2: forward, 5’-CCTTTGACCAGATGAACGGAGTG-3’; reverse, 5’-CTG GTTTCTAGGTGCAGAGATGG-3’; and cMyc: forward, 5’-CTT CTCTCCGTCCTCGGATTCT-3’; reverse, 5’-GAAGGTGATCCA GACTCTGACCTT-3’. Data were normalized to GAPDH (forward, 5’-GGCAAATTCAACGGCACAGT-3’; reverse, 5’-GATGGTGAT GGGCTTCCC-3’).

RNaseq

RNA was extracted from sorted cells using an RNeasy Mini Kit (Qiagen). Total RNA samples were mixed with oligo-dT and dNTPs, incubated at 72°C, and immediately put back on ice. Reverse transcription into cDNA was performed based on polyA tail, followed by template switch at the 5’ end of the RNA and amplification of the full-length cDNA by PCR. The average molecule length was analyzed using the Agilent Technologies 2100 bioanalyzer instrument. For library construction, PCR products were purified and selected with the Agencourt AMPure XP-Medium kit. DNA was quantified by Agilent Technologies 2100 bioanalyzer. Double-stranded PCR products were the heat denatured and circularized by the splint oligo sequence. Single-stranded circle DNA was formatted as the final library. The library was amplified to make DNA nanoball, which had more than 300 copies of one molecule. DNA nanoballs were loaded into the patterned nanoarray and single-end 50-base reads were generated in the way of sequenced by combinatorial Probe-Anchor Synthesis. The RNaseq data underwent thorough quality control with FastQC and MultiQC, ([Ewels et al., 2016](#)) before sequencing adapter trimming was performed with trim-galore. Read mapping and quantification was performed with Salmon ([Patro et al., 2017](#)) using the Gencode ([Frankish et al., 2019](#)) mouse reference transcriptome vM23. The Salmon quasi-index

was created with a default k-mer length of 31 and the Gencode flag. Subsequent quantification was performed while accounting for sequence-specific biases, like random hexamer priming, which often results in lower base-call quality of the first few bases of a read. Additional parameters included `--validateMappings` and `--rangeFactorizationBins 4` to potentially improve the quantification accuracy. Additionally, the `--gcBias` flag was used to correct for the slightly skewed GC content of the reads observed in the quality control step. The transcript counts were summarized to gene level with `tximport` (Soneson et al., 2015) and supplementary annotation data from Ensembl (Zerbino et al., 2018) through the `biomaRt` package (Durinck et al., 2005; Durinck et al., 2009). During this summarization step, allosomal and mitochondrial genes were excluded to decrease (sex-specific) biases. Differential expression analysis was performed by DESeq2 (Love et al., 2014) on gene-level counts. The reported log fold changes were shrunk with `apeglm` (Zhu et al., 2019). Gene-set enrichment analysis was performed for the DE genes with `goseq` (Young et al., 2010) both for Gene Ontology (Ashburner et al., 2000; The Gene Ontology Consortium, 2019) terms and Kyoto Encyclopedia of Genes and Genomes (Kanehisa and Goto, 2000; Kanehisa et al., 2019) pathways. The P values of the enrichment analyses were multiple testing corrected and a significance threshold of false discovery rate < 0.05 was used to determine the terms and pathways with a significantly altered number of DE genes. The transcriptomic data in this publication have been deposited in the National Center for Biotechnology Information Gene Expression Omnibus and are accessible through accession no. GSE171989. All original data are accessible through the corresponding author upon reasonable request.

Liquid chromatography-tandem mass spectrometry-based lipid mediator metabololipidomics

Samples were extracted and lipid mediators were identified and quantified as described (Gomez et al., 2020). In brief, tissues were placed in 1 ml of ice-cold methanol containing deuterated internal standards (d_8 -5S-HETE, d_4 -LTB₄, d_5 -LXA₄, d_4 -PGE₂, d_5 -RvD2, d_5 -MaR1, d_5 -MaR2, d_5 -RvD3, d_4 -RvE1, d_5 -17R-RvD1, d_5 -LTC₄, d_5 -LTD₄, and d_5 -LTE₄) representing each chromatographic region of identified lipid mediator. Following protein precipitation (-20°C for a minimum of 45 min), supernatants were extracted on an ExtraHera instrument (Biotage) using solid-phase extraction with Isolute C18 500-mg columns (Biotage). Methyl formate and methanol fractions were collected, brought to dryness, and resuspended in phase (methanol:water, 1:1 vol/vol) for injection on a Shimadzu LC-20AD HPLC and a Shimadzu SIL-20AC autoinjector, paired with a QTrap 5500 or QTrap 6500+ (Sciex). In the analysis of mediators eluted in the methyl formate fraction, an Agilent Poroshell 120 EC-C18 column (100 mm \times 4.6 mm \times 2.7 μm) was kept at 50°C and mediators eluted using a mobile phase consisting of methanol:water:acetic acid of 20:80:0.01 (vol/vol/vol) that was ramped to 50:50:0.01 (vol/vol/vol) over 0.5 min and then to 80:20:0.01 (vol/vol/vol) from 2 min to 11 min, maintained until 14.5 min and then rapidly ramped to 98:2:0.01 (vol/vol/vol) for the next 0.1 min. This was subsequently maintained at 98:2:0.01 (vol/vol/vol) for 5.4 min,

and the flow rate was maintained at 0.5 ml/min. QTrap 5500 was operated in negative ionization mode using a multiple reaction monitoring method. In the analysis of mediators eluted in the methanol fraction, an Agilent Poroshell 120 EC-C18 column (100 mm \times 4.6 mm \times 2.7 μm) was kept at 50°C and mediators were eluted using a mobile phase consisting of methanol:water:acetic acid 55:45:0.5 (vol/vol/vol) over 5 min, ramped to 80:20:0.5 (vol/vol/vol) for 2 min, maintained at 80:20:0.5 (vol/vol/vol) for the successive 3 min, and ramped to 98:2:0.5 (vol/vol/vol) over 3 min. This condition was kept for 3 min. QTrap 6500+ was operated in positive ionization mode using a multiple reaction monitoring method. Each lipid mediator was identified using established criteria, including: (1) the presence of a peak with a minimum area of 2,000 counts, (2) matching retention time to synthetic or authentic standards, (3) four or more data points, and (4) matching of at least six diagnostic ions to that of the reference standard, with a minimum of one backbone fragment being identified. Calibration curves were obtained for each mediator using synthetic compound mixtures at 0.78, 1.56, 3.12, 6.25, 12.5, 25, 50, 100, and 200 pg that gave linear calibration curves with r^2 values of 0.98–0.99. The results of the lipid mediator quantification in mouse lung tissue are presented in Table S1. The original raw data are accessible through the corresponding author upon reasonable request.

Statistics

Statistical analysis was performed with SPSS (version 22.0) using Mann-Whitney test where appropriate. More than two groups were compared using one-way ANOVA followed by Bonferroni testing. Data distribution was assessed using Kolmogorov-Smirnov test or Shapiro-Wilks test. All data are represented as whisker box pots with 25th to 75th percentile (interquartile ranges). A P value < 0.05 was considered significant. For in vivo experiments, the provided n is the number of animals used per experiment.

Online supplemental material

Fig. S1, related to Fig. 1, shows MIP2 α serum levels and systemic platelet and leukocyte count after injection of platelet-depleting antibody, platelet depletion scheme, erythrocytes, and white blood cell counts in peripheral blood of PF4^{+/+}iDTR mice after control and DT treatment, survival analysis, and lung wet/dry ratios. Fig. S2, related to Figs. 1, 2, 3, and 5, shows exemplary flow cytometry plots and gating strategy of lung homogenates, platelet-neutrophil aggregates, apoptosis rates in CD41^{neg} (without bound platelet), and CD41^{pos} (with bound platelet) neutrophils and P-selectin surface expression on platelets. Fig. S3, related to Figs. 3, 4, and 5, shows a scheme of T reg cell depletion and T reg cell and PMN counts in DERE mice, exemplary images from platelet-spreading experiments, and a scheme of PMN depletion and PMN counts in Mrp8-iDTR mice. Fig. S4, related to Fig. 4, shows data from bacterial pneumonia in CD40L^{-/-} mice and mice treated with blocking antibodies against CD40 and P-selectin. Fig. S5, related to Fig. 6, shows monocyte recruitment from the circulation into the lung during resolution, data on the effect of macrophage depletion on the resolution of bacterial pneumonia, and concentrations of TNF α

and IFN γ in the BAL supernatant. Table S1 lists the results of the lipid mediator quantification in mouse lung tissue.

Data availability

The transcriptomic data in this publication have been deposited in the National Center for Biotechnology Information Gene Expression Omnibus and are accessible through accession no. [GSE171989](https://www.ncbi.nlm.nih.gov/geo/query/acc.cgi?acc=GSE171989). All original data are accessible through the corresponding author upon reasonable request.

Acknowledgments

This work was supported by Deutsche Forschungsgemeinschaft grants ZA428/14-1, INST 211/604-2, Za2/001/18, RO4537/3-1, RO4537/4-1, RO4537/5-1, and KFO342 and the German-Israeli Foundation for Scientific Research and Development (grant I-1470-412.13/2018).

Author contributions: J. Rossaint: Conceived of the study, performed the experiments, analyzed the data, and wrote the manuscript; K. Thomas, S. Mersmann, J. Skupski, and A. Margraf: Performed experiments; T. Tekath: Performed biostatistical analysis; C. C. Jouvencé and J. Dalli: Performed lipid mediator analysis. A. Hidalgo, S.G. Meuth, O. Soehnlein, and A. Zarbock: Conceived of the study, analyzed the data, and contributed to writing the manuscript.

Disclosures: J. Dalli reported "other" from Resolomics Limited outside the submitted work. A. Zarbock reported grants from Deutsche Forschungsgemeinschaft during the conduct of the study. No other disclosures were reported.

Submitted: 26 June 2020

Revised: 29 October 2020

Accepted: 19 April 2021

References

Adrover, J.M., A. Aroca-Crevillén, G. Crainiciuc, F. Ostos, Y. Rojas-Vega, A. Rubio-Ponce, C. Cilloniz, E. Bonzón-Kulichenko, E. Calvo, D. Rico, et al. 2020. Programmed 'disarming' of the neutrophil proteome reduces the magnitude of inflammation. *Nat. Immunol.* 21:135-144. <https://doi.org/10.1038/s41590-019-0571-2>

Amison, R.T., B.G. O'Shaughnessy, S. Arnold, S.J. Cleary, M. Nandi, S.C. Pitchford, A. Bragonzi, and C.P. Page. 2018. Platelet Depletion Impairs Host Defense to Pulmonary Infection with *Pseudomonas aeruginosa* in Mice. *Am. J. Respir. Cell Mol. Biol.* 58:331-340. <https://doi.org/10.1165/rcmb.2017-0083OC>

Andonegui, G., C.S. Bonder, F. Green, S.C. Mullaly, L. Zbytniuk, E. Raharjo, and P. Kubes. 2003. Endothelium-derived Toll-like receptor-4 is the key molecule in LPS-induced neutrophil sequestration into lungs. *J. Clin. Invest.* 111:1011-1020. <https://doi.org/10.1172/JCI16510>

Ranieri, V.M., G.D. Rubenfeld, B.T. Thompson, N.D. Ferguson, E. Caldwell, E. Fan, L. Camporota, and A.S. Slutsky. ARDS Definition Task Force. 2012. Acute respiratory distress syndrome: the Berlin Definition. *JAMA.* 307:2526-2533.

Arienti, S., N.D. Barth, D.A. Dorward, A.G. Rossi, and I. Dransfield. 2019. Regulation of Apoptotic Cell Clearance During Resolution of Inflammation. *Front. Pharmacol.* 10:891. <https://doi.org/10.3389/fphar.2019.00891>

Ashburner, M., C.A. Ball, J.A. Blake, D. Botstein, H. Butler, J.M. Cherry, A.P. Davis, K. Dolinski, S.S. Dwight, J.T. Eppig, et al. The Gene Ontology Consortium. 2000. Gene ontology: tool for the unification of biology. *Nat. Genet.* 25:25-29. <https://doi.org/10.1038/75556>

Ashcroft, T., J.M. Simpson, and V. Timbrell. 1988. Simple method of estimating severity of pulmonary fibrosis on a numerical scale. *J. Clin. Pathol.* 41:467-470. <https://doi.org/10.1136/jcp.41.4.467>

Barth, N.D., J.A. Marwick, M. Vendrell, A.G. Rossi, and I. Dransfield. 2017. The "Phagocytic Synapse" and Clearance of Apoptotic Cells. *Front. Immunol.* 8:1708. <https://doi.org/10.3389/fimmu.2017.01708>

Benoit, M.E., E.V. Clarke, P. Morgado, D.A. Fraser, and A.J. Tenner. 2012. Complement protein C1q directs macrophage polarization and limits inflammasome activity during the uptake of apoptotic cells. *J. Immunol.* 188:5682-5693. <https://doi.org/10.4049/jimmunol.1103760>

Bergmann, C.B., F. Hefele, M. Unger, S. Huber-Wagner, P. Biberthaler, M. van Griensven, and M. Hanschen. 2016. Platelets modulate the immune response following trauma by interaction with CD4+ T regulatory cells in a mouse model. *Immunol. Res.* 64:508-517. <https://doi.org/10.1007/s12026-015-8726-1>

Bratton, D.L., and P.M. Henson. 2011. Neutrophil clearance: when the party is over, clean-up begins. *Trends Immunol.* 32:350-357. <https://doi.org/10.1016/j.it.2011.04.009>

Buch, T., F.L. Heppner, C. Tertilt, T.J. Heinen, M. Kremer, F.T. Wunderlich, S. Jung, and A. Waisman. 2005. A Cre-inducible diphtheria toxin receptor mediates cell lineage ablation after toxin administration. *Nat. Methods.* 2:419-426. <https://doi.org/10.1038/nmeth762>

Cilloniz, C., M. Ferrer, A. Liapikou, C. Garcia-Vidal, A. Gabarrus, A. Ceccato, J. Puig de La Bellacasa, F. Blasi, and A. Torres. 2018. Acute respiratory distress syndrome in mechanically ventilated patients with community-acquired pneumonia. *Eur. Respir. J.* 51:1702215. <https://doi.org/10.1183/13993003.02215-2017>

Cleary, S.J., C. Hobbs, R.T. Amison, S. Arnold, B.G. O'Shaughnessy, E. Le-françois, B. Mallavia, M.R. Looney, C.P. Page, and S.C. Pitchford. 2019. LPS-induced Lung Platelet Recruitment Occurs Independently from Neutrophils, PSGL-1, and P-Selectin. *Am. J. Respir. Cell Mol. Biol.* 61:232-243. <https://doi.org/10.1165/rcmb.2018-0182OC>

Davenpeck, K.L., M.E. Brummet, S.A. Hudson, R.J. Mayer, and B.S. Bochner. 2000. Activation of human leukocytes reduces surface P-selectin glycoprotein ligand-1 (PSGL-1, CD162) and adhesion to P-selectin in vitro. *J. Immunol.* 165:2764-2772. <https://doi.org/10.4049/jimmunol.165.5.2764>

Domínguez-Luis, M., A. Lamana, J. Vazquez, R. García-Navas, F. Mollinedo, F. Sánchez-Madrid, F. Díaz-González, and A. Urzainqui. 2011. The metalloprotease ADAM8 is associated with and regulates the function of the adhesion receptor PSGL-1 through ERM proteins. *Eur. J. Immunol.* 41:3436-3442. <https://doi.org/10.1002/eji.201141764>

Dong, J., J. Lin, B. Wang, S. He, C. Wu, K.K. Kushwaha, N. Mohabeer, Y. Su, H. Fang, K. Huang, and D. Li. 2015. Inflammatory cytokine TSLP stimulates platelet secretion and potentiates platelet aggregation via a TSLPR-dependent PI3K/Akt signaling pathway. *Cell. Physiol. Biochem.* 35:160-174. <https://doi.org/10.1159/000369684>

Doran, A.C., A. Yurdagul Jr., and I. Tabas. 2020. Efferocytosis in health and disease. *Nat. Rev. Immunol.* 20:254-267. <https://doi.org/10.1038/s41577-019-0240-6>

Drey Mueller, D., J. Pruessmeyer, J. Schumacher, S. Fellendorf, F.M. Hess, A. Seifert, A. Babendreyer, J.W. Bartsch, and A. Ludwig. 2017. The metalloproteinase ADAM8 promotes leukocyte recruitment in vitro and in acute lung inflammation. *Am. J. Physiol. Lung Cell. Mol. Physiol.* 313:L602-L614. <https://doi.org/10.1152/ajplung.00444.2016>

Durinck, S., Y. Moreau, A. Kasprzyk, S. Davis, B. De Moor, A. Brazma, and W. Huber. 2005. BioMart and Bioconductor: a powerful link between biological databases and microarray data analysis. *Bioinformatics.* 21:3439-3440. <https://doi.org/10.1093/bioinformatics/bti525>

Durinck, S., P.T. Spellman, E. Birney, and W. Huber. 2009. Mapping identifiers for the integration of genomic datasets with the R/Bioconductor package biomaRt. *Nat. Protoc.* 4:1184-1191. <https://doi.org/10.1038/nprot.2009.97>

Ehrentraut, H., E.T. Clambey, E.N. McNamee, K.S. Brodsky, S.F. Ehrentraut, J.M. Poth, A.K. Riegel, J.A. Westrich, S.P. Colgan, and H.K. Eltzschig. 2013. CD73+ regulatory T cells contribute to adenosine-mediated resolution of acute lung injury. *FASEB J.* 27:2207-2219. <https://doi.org/10.1096/fj.12-225201>

Elaïb, Z., F. Adam, E. Berrou, J.C. Bordet, N. Prévost, R. Bobe, M. Bryckaert, and J.P. Rosa. 2016. Full activation of mouse platelets requires ADP secretion regulated by SERCA3 ATPase-dependent calcium stores. *Blood.* 128:1129-1138. <https://doi.org/10.1182/blood-2015-10-678383>

Ewels, P., M. Magnusson, S. Lundin, and M. Källér. 2016. MultiQC: summarize analysis results for multiple tools and samples in a single report. *Bioinformatics.* 32:3047-3048. <https://doi.org/10.1093/bioinformatics/btw354>

- Fadok, V.A., D.L. Bratton, A. Konowal, P.W. Freed, J.Y. Westcott, and P.M. Henson. 1998. Macrophages that have ingested apoptotic cells in vitro inhibit proinflammatory cytokine production through autocrine/paracrine mechanisms involving TGF-beta, PGE2, and PAF. *J. Clin. Invest.* 101:890–898. <https://doi.org/10.1172/JCI1112>
- Frankish, A., M. Diekhans, A.M. Ferreira, R. Johnson, I. Jungreis, J. Loveland, J.M. Mudge, C. Sisu, J. Wright, J. Armstrong, et al. 2019. GENCODE reference annotation for the human and mouse genomes. *Nucleic Acids Res.* 47(D1):D766–D773. <https://doi.org/10.1093/nar/gky955>
- Gaertner, F., Z. Ahmad, G. Rosenberger, S. Fan, L. Nicolai, B. Busch, G. Yavuz, M. Luckner, H. Ishikawa-Ankerhold, R. Hennel, et al. 2017. Migrating Platelets Are Mechano-scavengers that Collect and Bundle Bacteria. *Cell.* 171:1368–1382.e23. <https://doi.org/10.1016/j.cell.2017.11.001>
- Gerdes, N., L. Zhu, M. Ersoy, A. Hermansson, P. Hjerdahl, H. Hu, G.K. Hansson, and N. Li. 2011. Platelets regulate CD4⁺ T-cell differentiation via multiple chemokines in humans. *Thromb. Haemost.* 106:353–362. <https://doi.org/10.1160/TH11-01-0020>
- Gomez, E.A., R.A. Colas, P.R. Souza, R. Hands, M.J. Lewis, C. Bessant, C. Pitzalis, and J. Dalli. 2020. Blood pro-resolving mediators are linked with synovial pathology and are predictive of DMARD responsiveness in rheumatoid arthritis. *Nat. Commun.* 11:5420. <https://doi.org/10.1038/s41467-020-19176-z>
- Grommes, J., and O. Soehnlein. 2011. Contribution of neutrophils to acute lung injury. *Mol. Med.* 17:293–307. <https://doi.org/10.2119/molmed.2010.00138>
- Grommes, J., J.E. Alard, M. Drechsler, S. Wantha, M. Mörgelin, W.M. Kuebler, M. Jacobs, P. von Hundelshausen, P. Markart, M. Wygrecka, et al. 2012. Disruption of platelet-derived chemokine heteromers prevents neutrophil extravasation in acute lung injury. *Am. J. Respir. Crit. Care Med.* 185:628–636. <https://doi.org/10.1164/rccm.201108-1533OC>
- Hasenberg, M., A. Köhler, S. Bonifatius, A. Jeron, and M. Gunzer. 2011. Direct observation of phagocytosis and NET-formation by neutrophils in infected lungs using 2-photon microscopy. *J. Vis. Exp.* 2011:2659. <https://doi.org/10.3791/2659>
- Haworth, O., M. Cernadas, R. Yang, C.N. Serhan, and B.D. Levy. 2008. Resolvin E1 regulates interleukin 23, interferon-gamma and lipoxin A4 to promote the resolution of allergic airway inflammation. *Nat. Immunol.* 9:873–879. <https://doi.org/10.1038/ni.1627>
- He, R., L. Li, Y. Kong, L. Tian, X. Tian, P. Fang, M. Bian, and Z. Liu. 2019. Preventing murine transfusion-related acute lung injury by expansion of CD4⁺ CD25⁺ FoxP3⁺ Tregs using IL-2/anti-IL-2 complexes. *Transfusion.* 59:534–544. <https://doi.org/10.1111/trf.15064>
- Herter, J.M., J. Rossaint, and A. Zarbock. 2014. Platelets in inflammation and immunity. *J. Thromb. Haemost.* 12:1764–1775. <https://doi.org/10.1111/jth.12730>
- Ittner, A., H. Block, C.A. Reichel, M. Varjosalo, H. Gehart, G. Sumara, M. Gstaiger, F. Krombach, A. Zarbock, and R. Ricci. 2012. Regulation of PTEN activity by p388-PKD1 signaling in neutrophils confers inflammatory responses in the lung. *J. Exp. Med.* 209:2229–2246. <https://doi.org/10.1084/jem.20120677>
- Jablonski, K.A., S.A. Amici, L.M. Webb, J.D. Ruiz-Rosado, P.G. Popovich, S. Partida-Sanchez, and M. Guerrou-de-Arellano. 2015. Novel Markers to Delineate Murine M1 and M2 Macrophages. *PLoS One.* 10:e0145342. <https://doi.org/10.1371/journal.pone.0145342>
- Kanehisa, M., and S. Goto. 2000. KEGG: kyoto encyclopedia of genes and genomes. *Nucleic Acids Res.* 28:27–30. <https://doi.org/10.1093/nar/28.1.27>
- Kanehisa, M., Y. Sato, M. Furumichi, K. Morishima, and M. Tanabe. 2019. New approach for understanding genome variations in KEGG. *Nucleic Acids Res.* 47(D1):D590–D595. <https://doi.org/10.1093/nar/gky962>
- Kapur, R., M. Kim, R. Aslam, M.J. McVey, A. Tabuchi, A. Luo, J. Liu, Y. Li, S. Shanmugabhavanathan, E.R. Speck, et al. 2017a. T regulatory cells and dendritic cells protect against transfusion-related acute lung injury via IL-10. *Blood.* 129:2557–2569. <https://doi.org/10.1182/blood-2016-12-758185>
- Kapur, R., M. Kim, J. Rebetz, M.T. Rondina, L. Porcelijn, and J.W. Semple. 2017b. Low levels of interleukin-10 in patients with transfusion-related acute lung injury. *Ann. Transl. Med.* 5:339. <https://doi.org/10.21037/atm.2017.04.37>
- Kapur, R., G. Kasetty, J. Rebetz, A. Egesten, and J.W. Semple. 2019. Osteopontin mediates murine transfusion-related acute lung injury via stimulation of pulmonary neutrophil accumulation. *Blood.* 134:74–84. <https://doi.org/10.1182/blood.2019000972>
- Kaur, M., T. Bell, S. Salek-Ardakani, and T. Hussell. 2015. Macrophage adaptation in airway inflammatory resolution. *Eur. Respir. Rev.* 24: 510–515. <https://doi.org/10.1183/16000617.0030-2015>
- Kennedy, A.D., and F.R. DeLeo. 2009. Neutrophil apoptosis and the resolution of infection. *Immunol. Res.* 43:25–61. <https://doi.org/10.1007/s12026-008-8049-6>
- Khandoga, A., M. Hanschen, J.S. Kessler, and F. Krombach. 2006. CD4⁺ T cells contribute to postischemic liver injury in mice by interacting with sinusoidal endothelium and platelets. *Hepatology.* 43:306–315. <https://doi.org/10.1002/hep.21017>
- Klann, J.E., S.H. Kim, K.A. Remedios, Z. He, P.J. Metz, J. Lopez, T. Tysl, J.G. Olvera, J.N. Ablack, J.M. Cantor, et al. 2018. Integrin Activation Controls Regulatory T Cell-Mediated Peripheral Tolerance. *J. Immunol.* 200: 4012–4023. <https://doi.org/10.4049/jimmunol.1800112>
- Kornerup, K.N., G.P. Salmon, S.C. Pitchford, W.L. Liu, and C.P. Page. 2010. Circulating platelet-neutrophil complexes are important for subsequent neutrophil activation and migration. *J Appl Physiol (1985).* 109:758–767. <https://doi.org/10.1152/jappphysiol.01086.2009>
- Lahl, K., and T. Sparwasser. 2011. In vivo depletion of FoxP3⁺ Tregs using the DREG mouse model. *Methods Mol. Biol.* 707:157–172. https://doi.org/10.1007/978-1-61737-979-6_10
- Lax, S., J. Rayes, S. Wichaiyo, E.J. Haining, K. Lowe, B. Grygielska, R. Laloo, P. Flodby, Z. Borok, E.D. Crandall, et al. 2017. Platelet CLEC-2 protects against lung injury via effects of its ligand podoplanin on inflammatory alveolar macrophages in the mouse. *Am. J. Physiol. Lung Cell. Mol. Physiol.* 313:L1016–L1029. <https://doi.org/10.1152/ajplung.00023.2017>
- Leitch, A.E., C.D. Lucas, J.A. Marwick, R. Duffin, C. Haslett, and A.G. Rossi. 2012. Cyclin-dependent kinases 7 and 9 specifically regulate neutrophil transcription and their inhibition drives apoptosis to promote resolution of inflammation. *Cell Death Differ.* 19:1950–1961. <https://doi.org/10.1038/cdd.2012.80>
- Levy, B.D., and C.N. Serhan. 2014. Resolution of acute inflammation in the lung. *Annu. Rev. Physiol.* 76:467–492. <https://doi.org/10.1146/annurev-physiol-021113-170408>
- Li, H., M.L. Edin, A. Gruzdev, J. Cheng, J.A. Bradbury, J.P. Graves, L.M. De-Graff, and D.C. Zeldin. 2013. Regulation of T helper cell subsets by cyclooxygenases and their metabolites. *Prostaglandins Other Lipid Mediat.* 104-105:74–83. <https://doi.org/10.1016/j.prostaglandins.2012.11.002>
- Lievens, D., A. Zernecke, T. Seijkens, O. Soehnlein, L. Beckers, I.C. Munnix, E. Wijnands, P. Goossens, R. van Kruchten, L. Thevissen, et al. 2010. Platelet CD40L mediates thrombotic and inflammatory processes in atherosclerosis. *Blood.* 116:4317–4327. <https://doi.org/10.1182/blood-2010-01-261206>
- Looney, M.R., J.X. Nguyen, Y. Hu, J.A. Van Ziffle, C.A. Lowell, and M.A. Matthay. 2009. Platelet depletion and aspirin treatment protect mice in a two-event model of transfusion-related acute lung injury. *J. Clin. Invest.* 119:3450–3461. <https://doi.org/10.1172/JCI38432>
- Love, M.I., W. Huber, and S. Anders. 2014. Moderated estimation of fold change and dispersion for RNA-seq data with DESeq2. *Genome Biol.* 15: 550. <https://doi.org/10.1186/s13059-014-0550-8>
- Lu, Y., Q. Li, Y.Y. Liu, K. Sun, J.Y. Fan, C.S. Wang, and J.Y. Han. 2015. Inhibitory effect of caffeic acid on ADP-induced thrombus formation and platelet activation involves mitogen-activated protein kinases. *Sci. Rep.* 5:13824. <https://doi.org/10.1038/srep13824>
- Matthay, M.A., L.B. Ware, and G.A. Zimmerman. 2012. The acute respiratory distress syndrome. *J. Clin. Invest.* 122:2731–2740. <https://doi.org/10.1172/JCI60331>
- Michaeloudes, C., P.K. Bhavsar, S. Mumby, B. Xu, C.K.M. Hui, K.F. Chung, and I.M. Adcock. 2020. Role of Metabolic Reprogramming in Pulmonary Innate Immunity and Its Impact on Lung Diseases. *J. Innate Immun.* 12:31–46. <https://doi.org/10.1159/000504344>
- Mitchell, S., G. Thomas, K. Harvey, D. Cottell, K. Reville, G. Berlasconi, N.A. Petasis, L. Erwig, A.J. Rees, J. Savill, et al. 2002. Lipoxins, aspirin-triggered epi-lipoxins, lipoxin stable analogues, and the resolution of inflammation: stimulation of macrophage phagocytosis of apoptotic neutrophils in vivo. *J. Am. Soc. Nephrol.* 13:2497–2507. <https://doi.org/10.1097/01.ASN.0000032417.73640.72>
- Ortiz-Muñoz, G., B. Mallavia, A. Bins, M. Headley, M.F. Krummel, and M.R. Looney. 2014. Aspirin-triggered 15-epi-lipoxin A4 regulates neutrophil-platelet aggregation and attenuates acute lung injury in mice. *Blood.* 124: 2625–2634. <https://doi.org/10.1182/blood-2014-03-562876>
- Patro, R., G. Duggal, M.I. Love, R.A. Irizarry, and C. Kingsford. 2017. Salmon provides fast and bias-aware quantification of transcript expression. *Nat. Methods.* 14:417–419. <https://doi.org/10.1038/nmeth.4197>
- Phillipson, M., and P. Kubes. 2011. The neutrophil in vascular inflammation. *Nat. Med.* 17:1381–1390. <https://doi.org/10.1038/nm.2514>
- Pitchford, S.C., S. Momi, S. Baglioni, L. Casali, S. Giannini, R. Rossi, C.P. Page, and P. Gresele. 2008. Allergen induces the migration of platelets to lung

- tissue in allergic asthma. *Am. J. Respir. Crit. Care Med.* 177:604–612. <https://doi.org/10.1164/rccm.200702-214OC>
- Potey, P.M., A.G. Rossi, C.D. Lucas, and D.A. Dorward. 2019. Neutrophils in the initiation and resolution of acute pulmonary inflammation: understanding biological function and therapeutic potential. *J. Pathol.* 247: 672–685. <https://doi.org/10.1002/path.5221>
- Rebetz, J., J.W. Semple, and R. Kapur. 2018. The Pathogenic Involvement of Neutrophils in Acute Respiratory Distress Syndrome and Transfusion-Related Acute Lung Injury. *Transfus. Med. Hemother.* 45:290–298. <https://doi.org/10.1159/000492950>
- Reutershan, J., A. Basit, E.V. Galkina, and K. Ley. 2005. Sequential recruitment of neutrophils into lung and bronchoalveolar lavage fluid in LPS-induced acute lung injury. *Am. J. Physiol. Lung Cell. Mol. Physiol.* 289: L807–L815. <https://doi.org/10.1152/ajplung.00477.2004>
- Rossaint, J., and A. Zarbock. 2015. Platelets in leucocyte recruitment and function. *Cardiovasc. Res.* 107:386–395. <https://doi.org/10.1093/cvr/cvv048>
- Rossaint, J., J.M. Herter, H. Van Aken, M. Napirei, Y. Döring, C. Weber, O. Soehnlein, and A. Zarbock. 2014. Synchronized integrin engagement and chemokine activation is crucial in neutrophil extracellular trap-mediated sterile inflammation. *Blood.* 123:2573–2584. <https://doi.org/10.1182/blood-2013-07-516484>
- Rossaint, J., K. Kühne, J. Skupski, H. Van Aken, M.R. Looney, A. Hidalgo, and A. Zarbock. 2016. Directed transport of neutrophil-derived extracellular vesicles enables platelet-mediated innate immune response. *Nat. Commun.* 7:13464. <https://doi.org/10.1038/ncomms13464>
- Rossi, A.G., D.A. Sawatzky, A. Walker, C. Ward, T.A. Sheldrake, N.A. Riley, A. Caldicott, M. Martinez-Losa, T.R. Walker, R. Duffin, et al. 2006. Cyclin-dependent kinase inhibitors enhance the resolution of inflammation by promoting inflammatory cell apoptosis. *Nat. Med.* 12:1056–1064. <https://doi.org/10.1038/nm1468>
- Semple, J.W., J. Rebetz, and R. Kapur. 2019. Transfusion-associated circulatory overload and transfusion-related acute lung injury. *Blood.* 133: 1840–1853. <https://doi.org/10.1182/blood-2018-10-860809>
- Setiady, Y.Y., J.A. Coccia, and P.U. Park. 2010. In vivo depletion of CD4+FOXP3+ Treg cells by the PC61 anti-CD25 monoclonal antibody is mediated by Fcγ3R+ phagocytes. *Eur. J. Immunol.* 40:780–786. <https://doi.org/10.1002/eji.200939613>
- Soneson, C., M.I. Love, and M.D. Robinson. 2015. Differential analyses for RNA-seq: transcript-level estimates improve gene-level inferences. *F1000 Res.* 4:1521. <https://doi.org/10.12688/f1000research.7563.1>
- Sreeramkumar, V., J.M. Adrover, I. Ballesteros, M.I. Cuartero, J. Rossaint, I. Bilbao, M. Náchter, C. Pitaval, I. Radovanovic, Y. Fukui, et al. 2014. Neutrophils scan for activated platelets to initiate inflammation. *Science.* 346:1234–1238. <https://doi.org/10.1126/science.1256478>
- The Gene Ontology Consortium. 2019. The Gene Ontology Resource: 20 years and still GOing strong. *Nucleic Acids Res.* 47(D1):D330–D338. <https://doi.org/10.1093/nar/gky1055>
- Wang, Y., Q. Shan, J. Pan, and S. Yi. 2018. Actin Cytoskeleton Affects Schwann Cell Migration and Peripheral Nerve Regeneration. *Front. Physiol.* 9:23. <https://doi.org/10.3389/fphys.2018.00023>
- Wuescher, L.M., A. Takashima, and R.G. Worth. 2015. A novel conditional platelet depletion mouse model reveals the importance of platelets in protection against *Staphylococcus aureus* bacteremia. *J. Thromb. Haemost.* 13:303–313. <https://doi.org/10.1111/jth.12795>
- Yadav, H., and D.J. Kor. 2015. Platelets in the pathogenesis of acute respiratory distress syndrome. *Am. J. Physiol. Lung Cell. Mol. Physiol.* 309: L915–L923. <https://doi.org/10.1152/ajplung.00266.2015>
- Yagnik, D. 2014. Macrophage derived platelet activating factor implicated in the resolution phase of gouty inflammation. *Int. J. Inflamm.* 2014: 526496. <https://doi.org/10.1155/2014/526496>
- Young, M.D., M.J. Wakefield, G.K. Smyth, and A. Oshlack. 2010. Gene ontology analysis for RNA-seq: accounting for selection bias. *Genome Biol.* 11:R14. <https://doi.org/10.1186/gb-2010-11-2-r14>
- Zarbock, A., K. Singbartl, and K. Ley. 2006. Complete reversal of acid-induced acute lung injury by blocking of platelet-neutrophil aggregation. *J. Clin. Invest.* 116:3211–3219. <https://doi.org/10.1172/JCI29499>
- Zerbino, D.R., P. Achuthan, W. Akanni, M.R. Amode, D. Barrell, J. Bhai, K. Billis, C. Cummins, A. Gall, C.G. Girón, et al. 2018. Ensembl 2018. *Nucleic Acids Res.* 46(D1):D754–D761. <https://doi.org/10.1093/nar/gkx1098>
- Zhu, A., J.G. Ibrahim, and M.I. Love. 2019. Heavy-tailed prior distributions for sequence count data: removing the noise and preserving large differences. *Bioinformatics.* 35:2084–2092. <https://doi.org/10.1093/bioinformatics/bty895>

Supplemental material

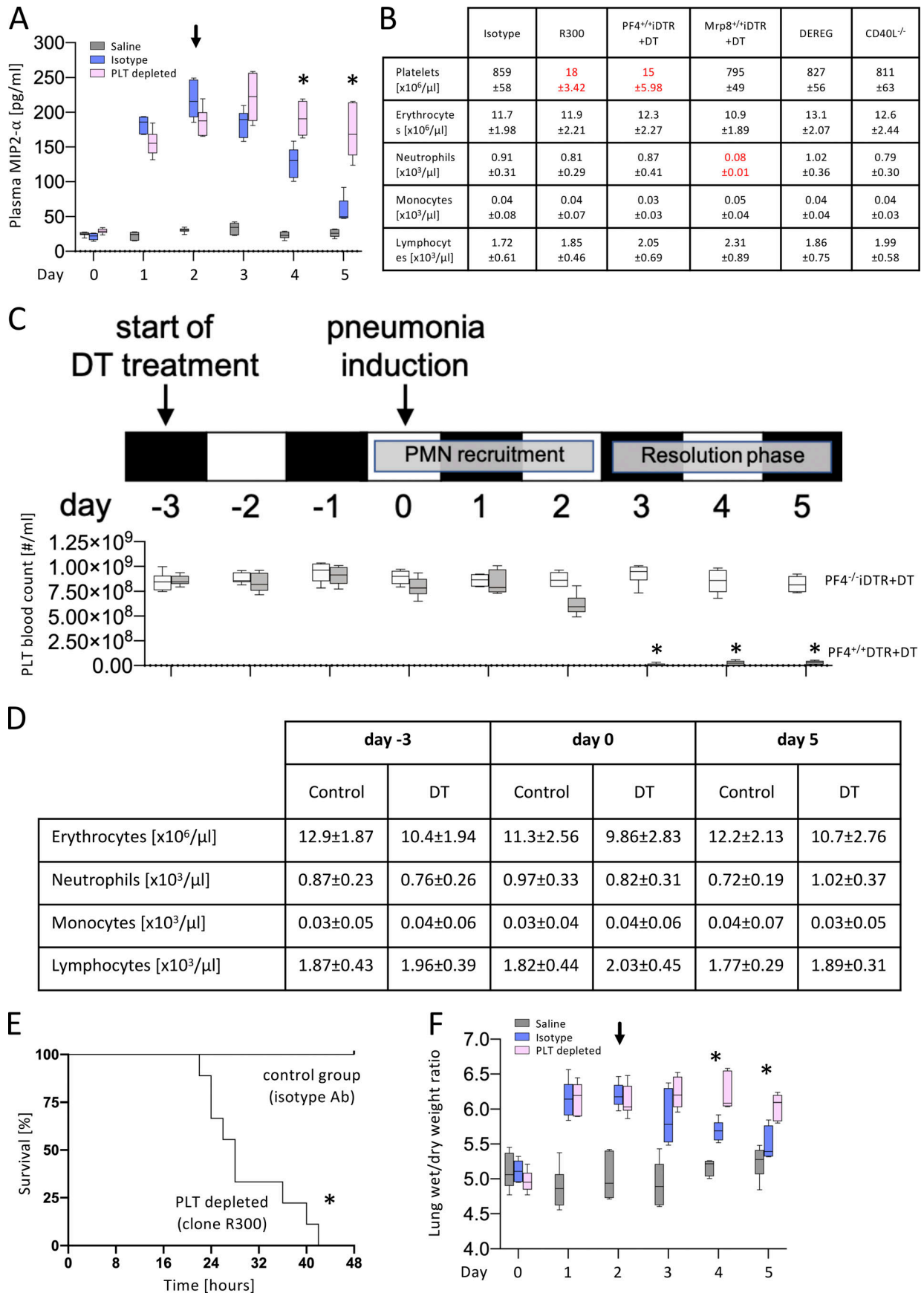


Figure S1. **Platelet depletion during bacterial pneumonia and in Pf4^{iDTR} mice.** **(A)** Bacterial pneumonia was induced in WT mice and MIP2 α serum levels were measured at the indicated time points by ELISA assays (data pooled from two independent experiments with four to six mice in each group; Mann-Whitney test was used for statistical analysis, *, $P < 0.05$). **(B)** Systemic platelet and leukocyte count after injection of platelet-depleting antibody (clone R300, 2 $\mu\text{g/g}$ body weight) or isotype control and in PF4^{+/+}iDTR+DT, Mrp8^{+/+}iDTR+DT, DEREK, and CD40L^{-/-} mice (data pooled from two independent experiments with four to six mice in each group; Mann-Whitney test was used for statistical analysis, *, $P < 0.05$). **(C)** Scheme of platelet depletion in PF4^{-/-}iDTR+DT and PF4^{+/+}iDTR+DT (receiving DT) mice and corresponding platelet counts (data pooled from two independent experiments with six mice in each group; Mann-Whitney test was used for statistical analysis, *, $P < 0.05$). **(D)** Erythrocytes and white blood cell counts in peripheral blood of PF4^{+/+}iDTR mice after control and DT treatment (data pooled from two independent experiments with four to six mice in each group; Mann-Whitney test was used for statistical analysis, *, $P < 0.05$). **(E)** Platelets were depleted by injection of a platelet-depleting antibody (clone R300, 2 $\mu\text{g/g}$ body weight) 1 d before induction of bacterial pneumonia and survival was analyzed by Kaplan-Meier plot for the following 48 h (data pooled from three independent experiments with 8–10 mice in each group; Kaplan-Meier survival analysis was used for statistical testing, *, $P < 0.05$). **(F)** Bacterial pneumonia was induced in WT or PF4-iDTR mice by i.t. instillation of viable *K. pneumoniae* (1.5×10^7 CFUs/mouse). Platelets were depleted 2 d after induction of pneumonia and the lung wet/dry ratio was analyzed (data pooled from two independent experiments with four to six mice in each group; Mann-Whitney test was used for statistical analysis, *, $P < 0.05$). Arrows in A and F indicate time point of platelet depletion.

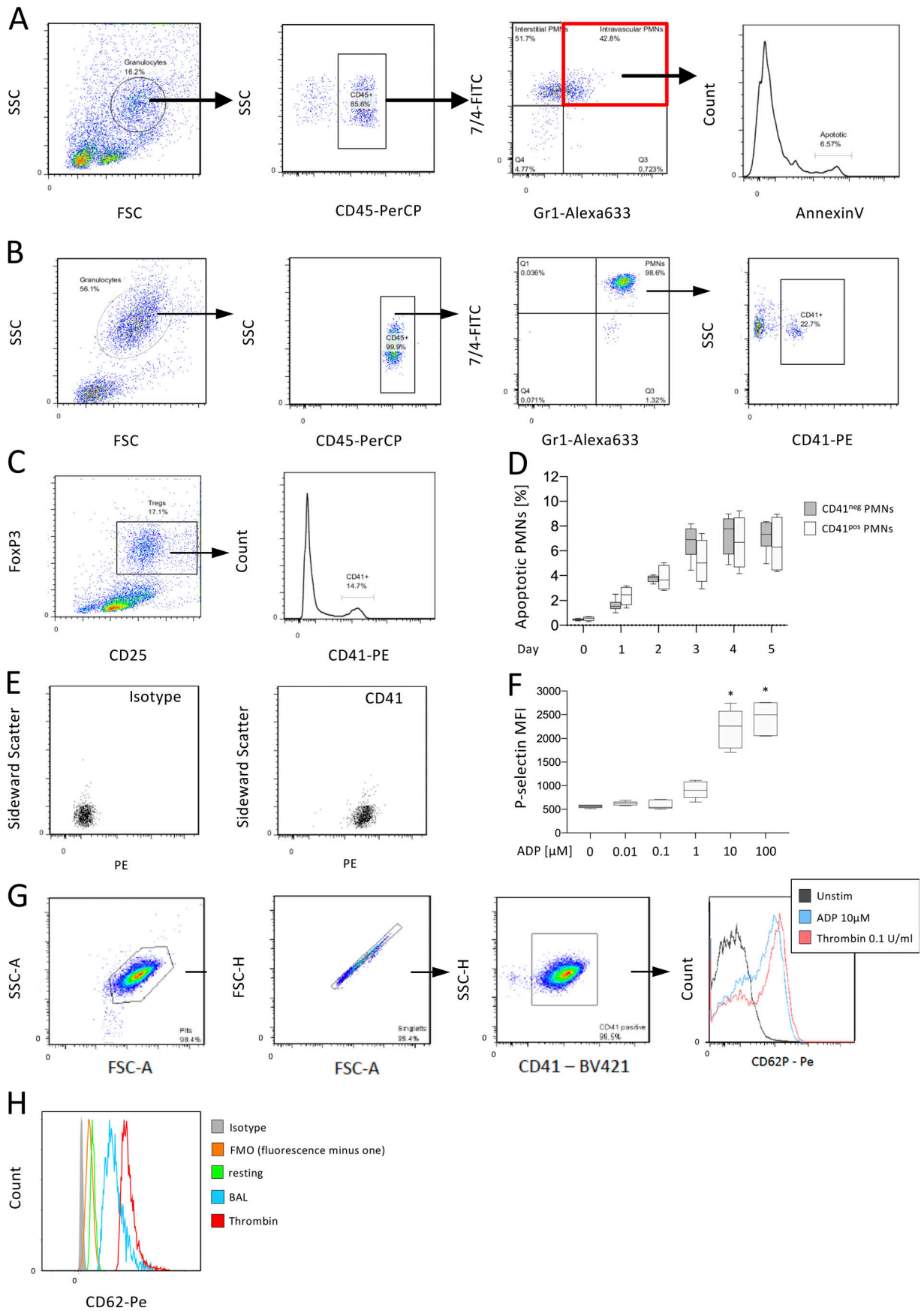


Figure S2. **Analysis of apoptotic neutrophils in the different lung compartments, platelet–leukocyte aggregates in the blood, and the BAL by flow cytometry.** **(A)** Exemplary flow cytometry plots and gating strategy of lung homogenates. **(B and C)** Exemplary flow cytometry plots and gating strategy of (B) platelet–neutrophil aggregates and (C) platelet–T reg cell aggregates. **(D)** Apoptosis rate in CD41^{neg} (without bound platelet) and CD41^{pos} (with bound platelet) neutrophil subpopulation in the BAL obtained from WT mice after induction of bacterial pneumonia (data pooled from two independent experiments with four to five mice in each group; Mann-Whitney test was used for statistical analysis, *, $P < 0.05$). **(E)** Platelets in the BAL fluid were analyzed by flow cytometry after induction of pneumonia (exemplary flow cytometry plots). Isolated WT platelets were stimulated with different ADP concentrations and platelet P-selectin surface expression was analyzed by flow cytometry. **(F and G)** Quantitative comparison of mean fluorescence intensity (MFI; F) and gating strategy and histogram of CD62-PE binding (G; data pooled from three independent experiments with six samples in each group; Mann-Whitney test was used for statistical analysis, *, $P < 0.05$). **(H)** BAL was obtained 3 d after induction of bacterial pneumonia in WT mice and platelets CD62-PE binding was analyzed and compared with resting and thrombin-stimulated WT platelets isolated from peripheral blood by flow cytometry (exemplary FACS plot from four experiments). FMO, fluorescence minus one sample of corresponding BAL sample; FSC, forward scatter; SSC, side scatter.

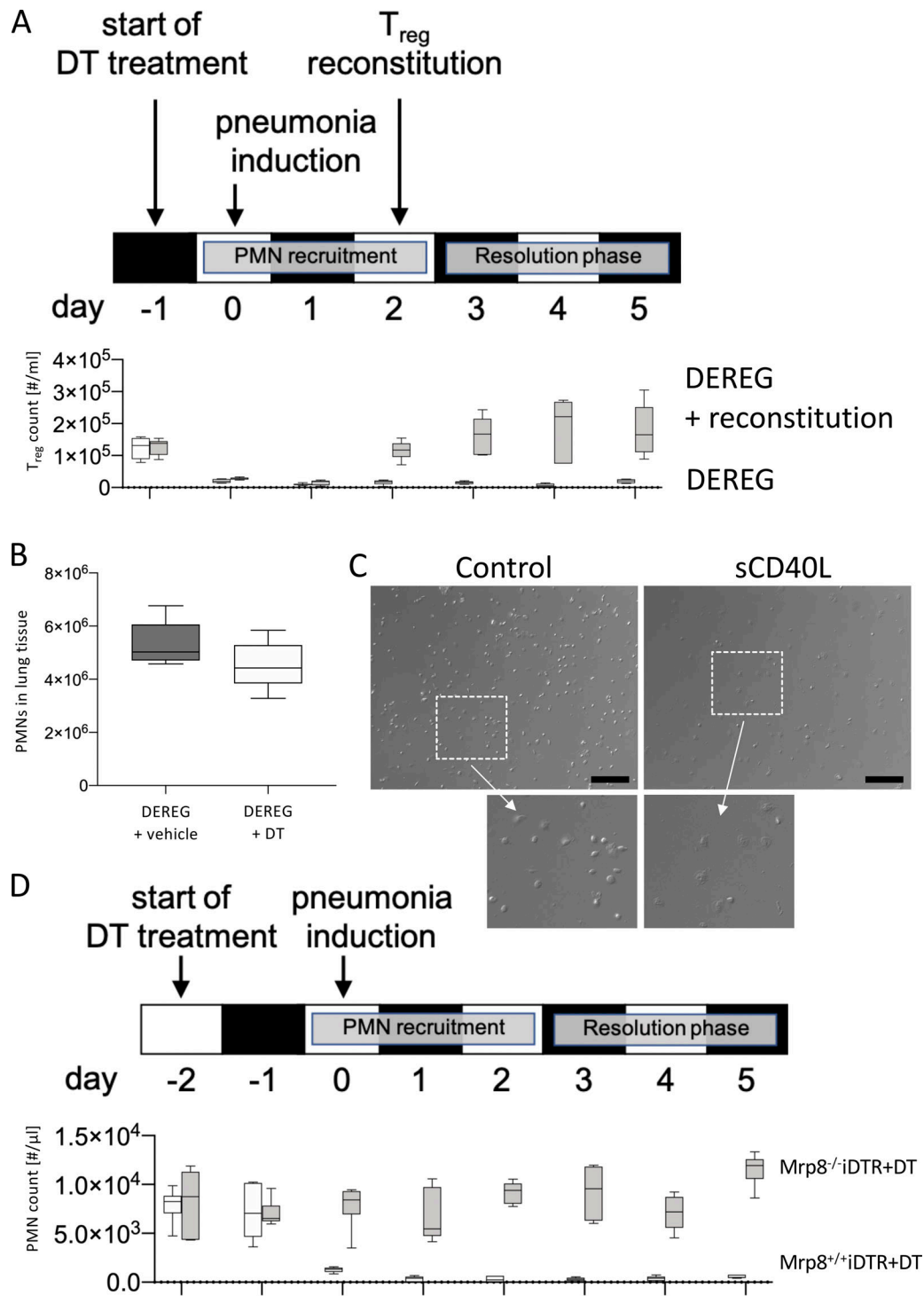


Figure S3. **T_{reg} cell depletion and reconstitution in DERE mice and neutrophil depletion in *Mrp8*^{+/+}iDTR mice.** (A) DERE mice were treated with 1 μ g DT i.p. and the T_{reg} cell count was analyzed daily. Some mice were reconstituted with isolated T_{reg} cells without iDTR at day 2 (data pooled from two independent experiments with 5–6 mice in each group; Mann-Whitney test was used for statistical analysis, *, P < 0.05). (B) DERE mice were treated with 1 μ g DT i.p. or vehicle control pulmonary neutrophil content after flushing out the pulmonary vasculature was analyzed at day 5 (data pooled from two independent experiments with five mice in each group; Mann-Whitney test was used for statistical analysis, *, P < 0.05). (C) WT platelets were incubated with vehicle or sCD40L (20 ng/ml) in vitro and platelet shape change after sCD40L stimulation was analyzed by light microscopy (exemplary images from three independent experiments with three samples in each group). Scale bar, 20 μ m; lower inserts provide higher magnification of designated area. (D) *Mrp8*^{+/+}iDTR and *Mrp8*^{-/-}iDTR mice were treated with 1 μ g DT i.p. and the neutrophil count in peripheral blood was analyzed daily (data pooled from two independent experiments with 5–6 mice in each group; Mann-Whitney test was used for statistical analysis, *, P < 0.05).

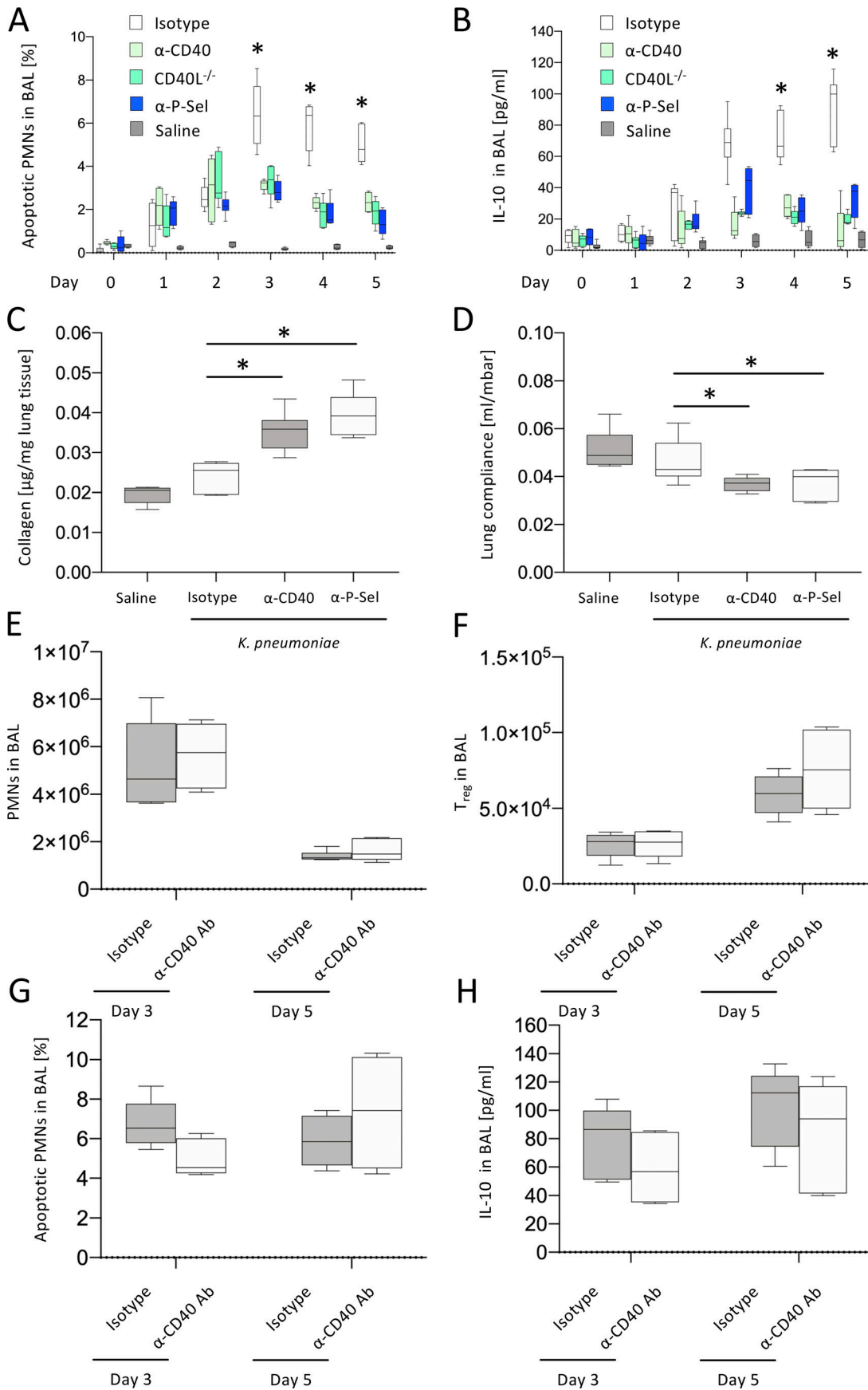


Figure S4. **CD40/CD40L is required for resolution of pulmonary inflammation.** Bacterial pneumonia was induced in WT mice and CD40L^{-/-} mice by i.t. instillation of viable *K. pneumoniae* (1.5×10^7 CFUs/mouse). Some WT mice received Fab fragments of blocking antibodies against P-selectin (clone RB40.34, 50 μ g/mouse), CD40 (clone HM40-3, 50 μ g/mouse i.v.), or isotype control 2 d after induction of pneumonia. **(A)** The percentage of apoptotic neutrophils in the BAL was analyzed by flow cytometry (data pooled from two independent experiments with four to six mice in each group; Mann-Whitney test was used for statistical analysis, *, $P < 0.05$). **(B)** The concentration of the cytokine IL-10 in the BAL fluid was analyzed by ELISA (data pooled from two independent experiments with four to six mice in each group; Mann-Whitney test was used for statistical analysis, *, $P < 0.05$). **(C and D)** 14 d after induction of pneumonia, **(C)** lung collagen content (estimated by measuring the absorbance of oxidized hydroxyproline in lung tissue homogenisates) and **(D)** lung compliance were analyzed (data pooled from three independent experiments with four to five mice in each group; Mann-Whitney test was used for statistical analysis, *, $P < 0.05$). Bacterial pneumonia was induced in WT mice by i.t. instillation of viable *K. pneumoniae* (1.5×10^7 CFUs/mouse). Mice received blocking antibodies against CD40 (clone HM40-3, 50 μ g/mouse i.v.) isotype control before induction of pneumonia. **(E-G)** At days 3 and 5, the number of **(E)** neutrophils and **(F)** T reg cells in the BAL fluid, and **(G)** the percentage of apoptotic neutrophils in the BAL were analyzed by flow cytometry (data pooled from two independent experiments with four to five mice in each group; Mann-Whitney test was used for statistical analysis, *, $P < 0.05$). **(H)** The concentration of IL-10 in the BAL was analyzed by ELISA (data pooled from two independent experiments with four to five mice in each group; Mann-Whitney test was used for statistical analysis, *, $P < 0.05$).

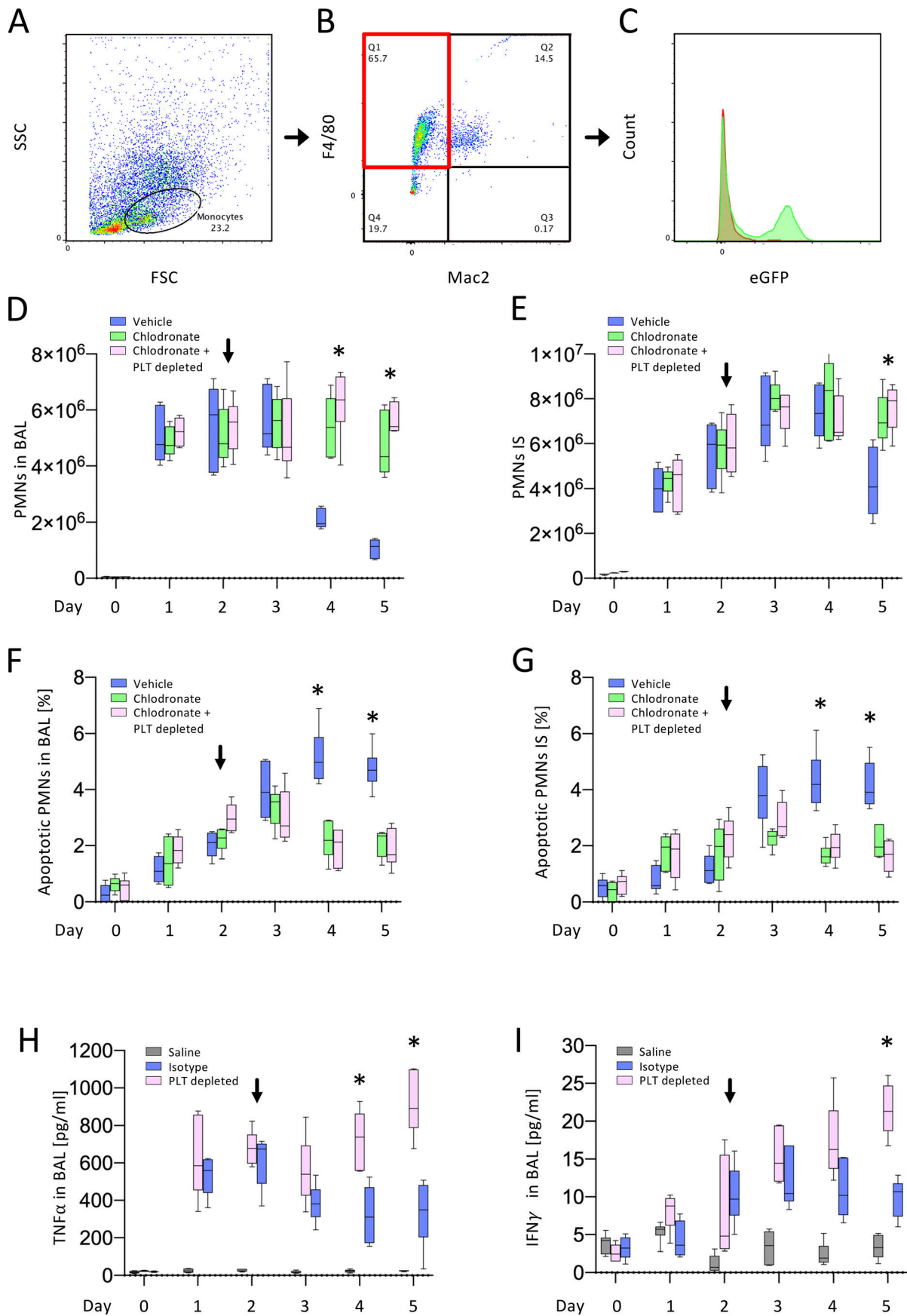


Figure S5. **Monocytes are recruited from the circulation into the lung during resolution.** Bacterial pneumonia was induced by i.t. instillation of viable *K. pneumoniae* in eGFP⁻ WT mice. Mice were injected with isolated monocytes from eGFP⁺ or eGFP⁻ donor mice. 5 d after induction of pneumonia, mice were sacrificed and BAL fluid was harvested for flow cytometry analysis. **(A and B)** Monocytes/macrophages in BAL fluid were identified by (A) native side scatter (SSC)/forward scatter (FSC) gating and (B) expression of F4/80. **(C)** Expression of GFP in the F4/80⁺ cell population in WT mice that were injected with monocytes from eGFP⁻ (control, red) or eGFP⁺ (green) donor mice (exemplary flow cytometry plots from two independent experiments with five mice per group). Macrophage depletion was performed by injection of chlodronate liposomes. Bacterial pneumonia was induced in control mice and macrophage-depleted mice by i.t. instillation of viable *K. pneumoniae* (1.5×10^7 CFUs/mouse). **(D–G)** The number of neutrophils in the BAL fluid (D) and interstitial compartment (IS; E), and the percentage of apoptotic neutrophils in the BAL (F) and interstitial compartment (G) was analyzed by flow cytometry (data pooled from two independent experiments with four to six mice in each group; Mann-Whitney test was used for statistical analysis, *, $P < 0.05$). BAL supernatant was obtained on day 5 from control mice and mice in which intravascular platelets were depleted by i.v. injection of a platelet-depleting antibody (clone R300, 2 μ g/g bodyweight) 2 d after induction of pneumonia. **(H and I)** Concentrations of TNF α (H) and IFN γ (I) in the supernatant were analyzed by ELISA assays (data pooled from two independent experiments with four to five mice in each group; Mann-Whitney test was used for statistical analysis, *, $P < 0.05$). Arrows indicate time point of platelet depletion.

Table S1 is provided online and shows the lipid mediator profiling report for *K. pneumoniae*-induced mouse lung injury with and without platelet-depleting antibody.